MODERN CONTROL DESIGN FOR A VARIABLE DISPLACEMENT HYDRAULIC PUMP

A thesis presented to the faculty of the Graduate School
University of Missouri-Columbia

In Partial Fulfillment
Of the Requirements for the Degree
Master of Science

By

PATRICK DEAN

Dr. Roger Fales, Thesis Supervisor

August 2006

The undersigned, appointed by the dean of the Graduate School, have examined the project entitled

MODERN CONTROL DESIGN FOR A VARIABLE DISPLACEMENT HYDRAULIC PUMP

Presented by Patrick Dean

a candidate for the degree of Masters of Science

and hereby certify that in their opinion it is worthy of acceptance.

Dr. Roger Fales, Assistant Professor, Mechanical and Aerospace Engineering

---

Dr. Craig Kluever, Professor, Mechanical and Aerospace Engineering

---

Dr. Robert McLaren, Professor Emeritus, Electrical and Computer Engineering

ACKNOWLEDGEMENTS

First and foremost, I would like to thank Dr. Roger C. Fales for his guidance on this and many other projects. His work ethic and personal drive are things of legend, making him the perfect mentor for any individual interested in educating himself or others. I feel truly honored to have collaborated with him, and hope that someday I might achieve the level of expertise in my chosen field that he wields in the fields of fluid power and control.

I would like to thank my friend and colleague Eko Prasetiawan, whose interest and direction allowed this project to become everything it is today.

I would like to thank Dr. Craig Kluever for his instruction in both my undergraduate and graduate study. His desire to educate is inexhaustible and his ability is second to none.

I would like to thank Dr. Robert McLaren, for assisting in the refinement of this work and participating in my thesis committee.

I would like to thank my friend and colleague Brian Bax, who provided honesty when necessary, criticism when warranted, and laughter whenever.

Finally, I would like to thank my family for all their love and support. They have provided stronger shoulders to lean on than I could have ever thought possible. The last two years have been a rollercoaster, and I hope that this work is proof that hardship truly is the fire that forges the strongest steel.

TABLE OF CONTENTS

LIST OF FIGURES

LIST OF TABLES

NOMENCLATURE

Symbol	Description	Units
P_p	Pump pressure	Pa
P_C	Control pressure	Pa
A_p	Pump-side control cylinder area	m^3
A_c	Control-valve side control cylinder area	m^3
P_T	Tank pressure	Pa
Q_c	Flow through control valve	m^3/sec
V_C	Volume in control chamber	m^3
z	Control cylinder position	m
x	Control valve position	m
θ	Swash-plate position	radians
F_{sp}	Force exerted on the swash-plate	N
β	Fluid bulk modulus	GPa
τ_{sp}	Swash-plate torque	N-m
$\tau_{viscous}$	Torque caused by viscous friction	N-m
τ_{swivel}	Torque caused by swivel arm	N-m
l_{sp}	Swash-plate moment arm	m
J_{sp}	Swash-plate rotational moment of inertia	Nms^2
η_{vol}	Volumetric efficiency	-
η_{mech}	Mechanical efficiency	-
V_d	Volumetric displacement of the pump	m^3
K_l	Leakage coefficient	m^3/s/Pa
C_d	Discharge coefficient	-
ρ	Fluid density	kg/m^3

ABSTRACT

In this work modern control methods are used to design and analyze control methods for a variable-displacement hydraulic pump. More accurate uncertainty descriptions are derived by using a structured uncertainty model as opposed to an unstructured uncertainty model. The system studied includes one variable-displacement swash-plate hydraulic pump with a constant engine speed model. The input to the system is the current actuating the control valve position, while the system output is the discharge pressure of the pump. The established PID controller design lacked robustness, encouraging design of a two degrees-of-freedom control scheme. Frequency domain tests show robustness improvement over the classical PID control scheme. Time domain results show similar performance from both the PID controlled system and the two degrees-of-freedom controlled system. Time domain tests also show improved robustness to parametric variation from the modern control method, while system responses to large disturbances are similar among both the classical and modern control schemes.

Chapter 1

INTRODUCTION

Hydraulic system dynamics, in general, possess a great amount of variability. From changing parameters to input disturbances, the behavior of these systems tends to vary as operating conditions change. Because stability and performance are affected when the system dynamics change, a controller for a hydraulic system must include consideration of these changing conditions. In the past, classical control methods were designed with stability in mind, and only by experimentation could their performance robustness be verified. A trial-and-error process involving the tuning of the controller was required. System variation could only be considered if the uncertain condition could be replicated in these experiments. By utilizing modern control design techniques, a designer may take into account many more aspects of the system than previously considered. The uncertainty of a system due to variance within the plant can be directly calculated and the tradeoff between performance and stability can be shown graphically. This ability allows modern controllers to perform over a wider range of conditions, improving the dependability of machinery. By using H_∞ control design, greater performance is possible relative to classical control techniques. H_∞ design allows for optimization of control routines and greater flexibility in the tradeoff between performance and stability by shaping the maximum singular value of specific transfer functions.

Hydraulic systems are designed to ensure stability under all operating conditions, resulting in relatively conservative performance characteristics. By using

more advanced, higher-order controllers, the performance of a system can be improved without sacrifices in stability. A hydraulic pump is an excellent example of a hydraulic system in which performance sacrifices have been made to ensure stability. For this reason, it is a good application of robust modern control design methods. A hydraulic pump can possess large amounts of variance from several different sources, making it likely that performance can be improved by these methods while still maintaining a stable system. The classical control technique currently employed for this system, known as proportional, integral, and derivative control (PID), cannot take all of these uncertainties into account, making modern control an excellent alternative.

The method for characterizing the uncertainty in a system is important in modern control design. The uncertain parameters of a system can be analyzed as a whole or they can be analyzed individually. Individual analysis is more complicated but yields more accurate results. Analyzing the uncertainty as a group produces controllers that are less accurate and therefore too conservative.

1.1 Classic Control Design and Analysis Limitations

One of the main difficulties of classical control system analysis is the inability to look beyond the ideal system. Uncertainty and variance cannot be quantified under classical methods, making extensive machine testing the sole option in uncertainty research. Njabeleke et al. [1] showed that some measure of overall uncertainty could be derived from experimental results using hydraulic equipment; however, this uncertainty model represents a conservative measure of system variance. The choice

of an uncertainty model is a key to the successful design of modern controllers, and Shamma [2] showed mathematically that structured uncertainty provided an inherent increase in accuracy over unstructured uncertainty.

1.2 Modern Control in Hydraulic Systems

Many examples exist of research using modern control methods in hydraulic systems. H_∞ control techniques in a multiple-input, multiple-output hydraulic powertrain system were implemented by Zhang et al. [3], showing that H_∞ methods could produce robust controllers. While the methods utilized in multiple-input, multiple-output control differ from those in single-input, single-output control, the same algorithms hold for both cases. Modern control methods were successfully applied in a double inverted pendulum system regulated by hydraulic actuators by Fales et al. [4], [5]. This system also possesses multiple outputs. A single-input, single-output hydraulic system was studied by Njabeleke [1], controlling the velocity of a cylinder using modern control methods. This work also concluded that the controllers produced by modern control methods need not necessarily be of high order. The high-order dynamics of modern controllers is often considered a disadvantage over lower-order classical controllers. Model order reduction was used to ensure the feasibility of using these controllers in hydraulic systems.

1.3 Research Objectives

The objectives of this research are to model a variable displacement hydraulic pump from first principles and test data, analyze the uncertainty of the model using

linear methods, develop modern controllers to increase robustness and performance, and analyze these controllers in the frequency and time domains to verify these properties.

1.4 Thesis Outline

Chapter 2 will address the modeling of the hydraulic pump. First-principles modeling and assumptions are discussed, followed by the validation of the model using test data. This chapter also involves the linearization of the model. Chapter 3 discusses the idea of system uncertainty. Both lumped uncertainty and structured uncertainty are investigated. Chapter 4 introduces modern control techniques. Chapter 5 contains control design techniques, with pressure control being the main topic. After control design, analysis of the resulting controllers begins in Chapter 6 with frequency domain studies of the controlled system. Chapter 7 presents the time domain analysis of the controllers. The behavior of the simulated controlled system is of great interest. Finally, overall conclusions about the research, suggestions for solutions to the problem statement, limitations of H_∞ control and future work are presented in Chapter 8.

Chapter 2

Hydraulic Pump Modeling

2.1 First Principles Model

The model constructed to simulate the variable displacement hydraulic pump assembly consists of three sections: the displacement model, the pump model, and the load model. Each of these three sections is kept separate as a means of ensuring accuracy. The connection from the displacement model to the pump model represents pump flow. The connection from the pump model to the load model represents pump pressure. A schematic of this assembly is shown in Figure 1.

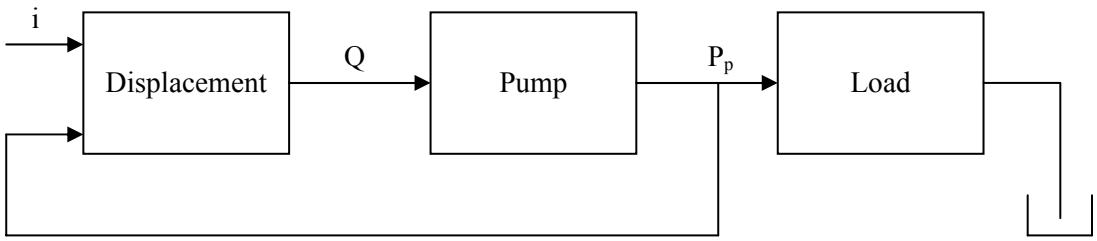

Figure 1. Schematic of the first principles model.

The test data describing this system that will eventually validate the model fits into this mold nicely. Data characterizing pump displacement as a function of input and pump pressure as a function of input exists, further encouraging this modeling strategy.

The displacement model was designed first. The inputs to the displacement model are the pump pressure (in Pa) and the pump command input (in Amps). The output of the displacement model is the pump flow rate (in cubic meters per second). The model itself consists of a control valve connected to a control chamber, which

directs the motion of the swash-plate. It also contains a swivel torque model, which affects the steady-state position of the swash-plate, and the dynamics of all moving parts within the system. The path of each input is summarized next.

The pump speed is involved in the calculation of the swivel torque. To simplify the problem, swivel torque is analyzed under a steady-state assumption for the swash-plate angular velocity. The swivel torque in a variable displacement swash-plate pump can be thought of as a torque either opposing or aiding the control cylinder's efforts to set the angle of the swash-plate. The swivel torque in this model is determined using a look-up table. The look-up table's inputs are the pump speed, the pump displacement, and the pump pressure. The exact figures of this look-up table will not be disclosed here, but overall, the swivel torque has a positive relationship with pump speed and displacement. This relationship means that, as the pump speed or the pump displacement increases, the swivel torque also increases.

After analyzing the steady-state characteristics of the swivel torque, the dynamic characteristics were modeled. The only dynamic effect on the swash-plate is the effect of viscous friction. The friction is determined by the pump pressure and the angular velocity of the swash-plate. The exact amount of torque that this friction exerts upon the swash-plate cannot be disclosed here, but the friction always opposes the movement of the swash plate, and the friction increases as the angular velocity of the swash-plate increases and as the pump pressure increases.

The pump pressure input to the displacement model has many different uses, just as the discharge pressure of a pump is used to regulate and control many different aspects of the system. One of the key uses of the pump pressure in pump control

centers on the control valve. This spool valve is used to regulate the pressure within the control chamber, which actuates the cylinder attached to the swash-plate, shown in Figure 2.

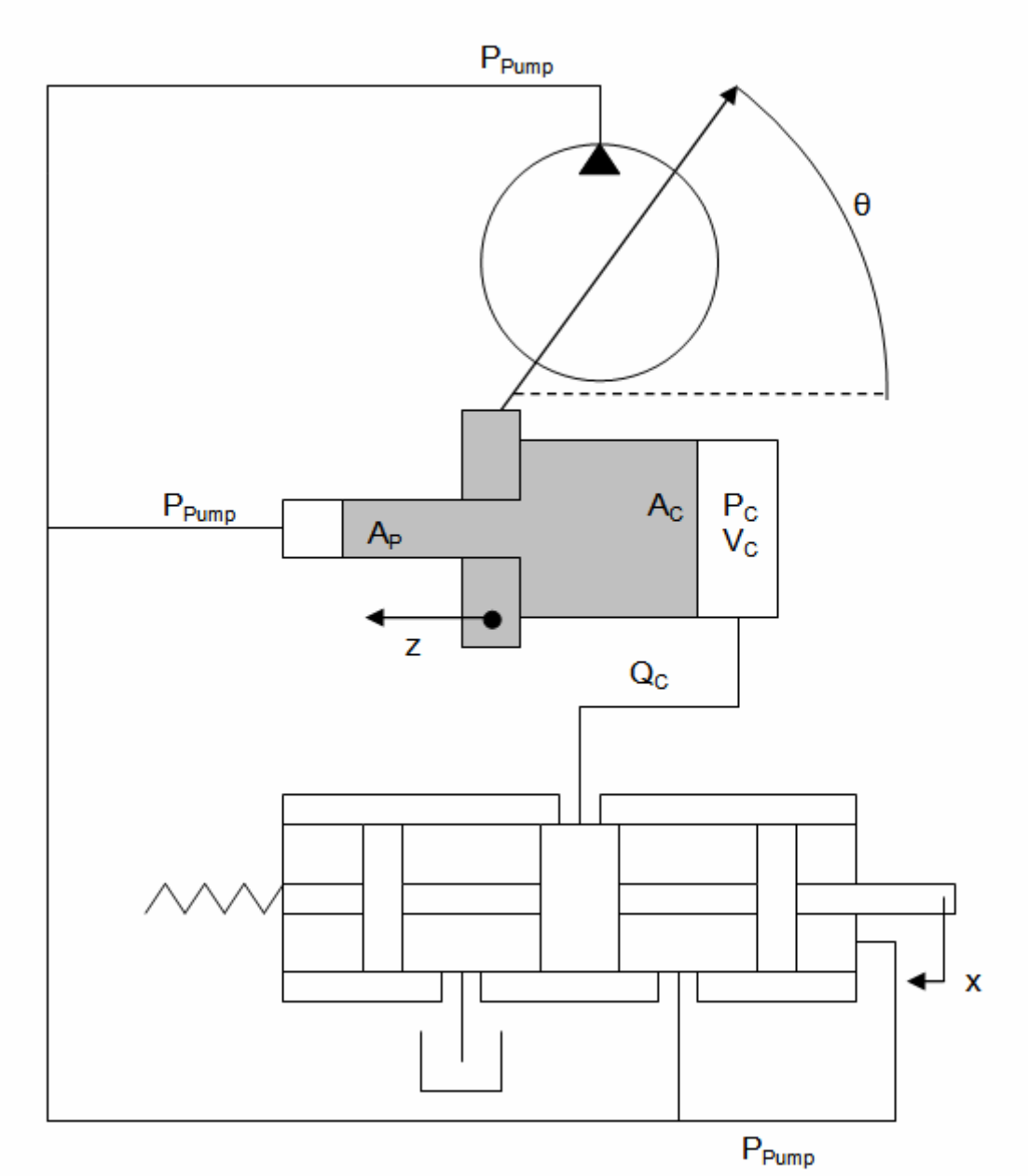

Figure 2. Pump schematic. Note that the position of the control cylinder (gray) dictates the displacement of the swash-plate.

To model the control valve in the pump, a decision had to be made. Either an analytical flow-force model of the valve could be used, taking into account the valve geometry and characteristics, or use of a table of flow information provided by the valve manufacturer. Due to the fact that 13 separate control valves had previously been constructed and tested, produced by three different manufacturers, and that data was readily available on all 13, the decision was made to use a table of flow information in lieu of a flow-force model. The advantage of this method was that tables could easily be changed in the system model to simulate different valves being used to control the swash-plate in the pump. The ability to introduce uncertainty into the system by using different control valves will be useful later when analyzing the system uncertainty.

The control valve used in the pump is a three-way spool valve with asymmetric porting angles. The port that connects the valve to the supply pressure is set at an angle relative to the other two ports, as shown in Figure 3. This port is known as the failure port. If the system were to lose electrical power, the resetting spring in the valve would force the spool to the end-stop, allowing full flow from the pump to reach the actuator chamber. This action fully displaces the swash plate, forcing the pump to achieve maximum pressure and flow. The reason for this design choice is due to the fact that in an excavator, for example, if the pump were forced to operate at maximum flow and pressure with no control, the system would still be operable using the control valves for each load. The disadvantage of this situation is that the system would then operate quite inefficiently, with a large pressure drop across each load valve.

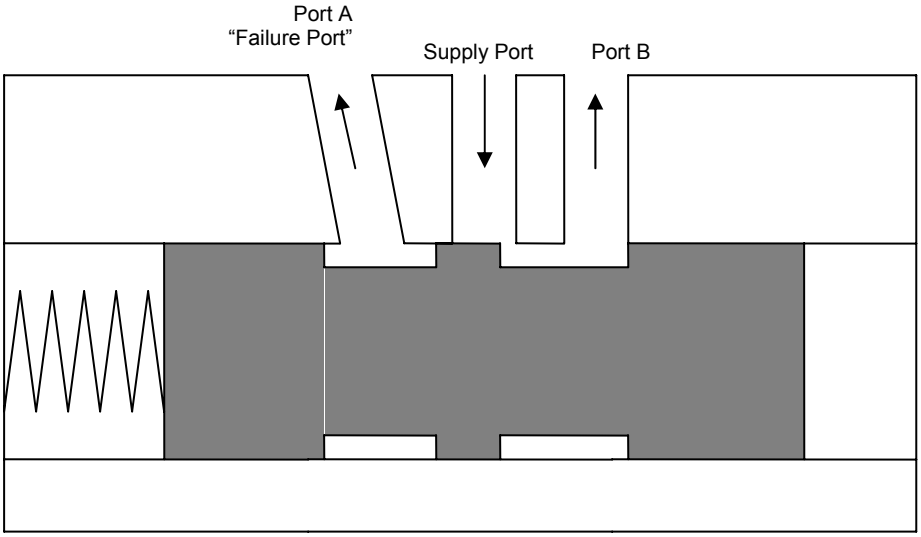

Figure 3. Schematic of spool valve with asymmetric porting.

The control valve data acquired from the valve manufacturers was incomplete. Each valve, individually, was to be tested by the manufacturers at four different supply pressures (1.5 MPa, 10 MPa, 20 MPa, and 30 MPa) and at a variety of input currents ranging from 0 A to 1.75 A. The parameter measured for each valve was the flow rate through the valve under each test condition. The problem was due to the fact that many of the data sets lacked information for one of the two output ports. In some data sets, there was no information given for the flow rate through the failure port, while in other sets, information was lacking for port B. An example of an erroneous and incomplete data set for a single pressure drop is shown in Figure 4. For comparison, a set of complete data for several pressure drops is shown in Figure 5. In these data sets, the flow measured for an input current less than 1 A signifies flow through the failure port while flow for an input current greater than 1 A passes through port B.

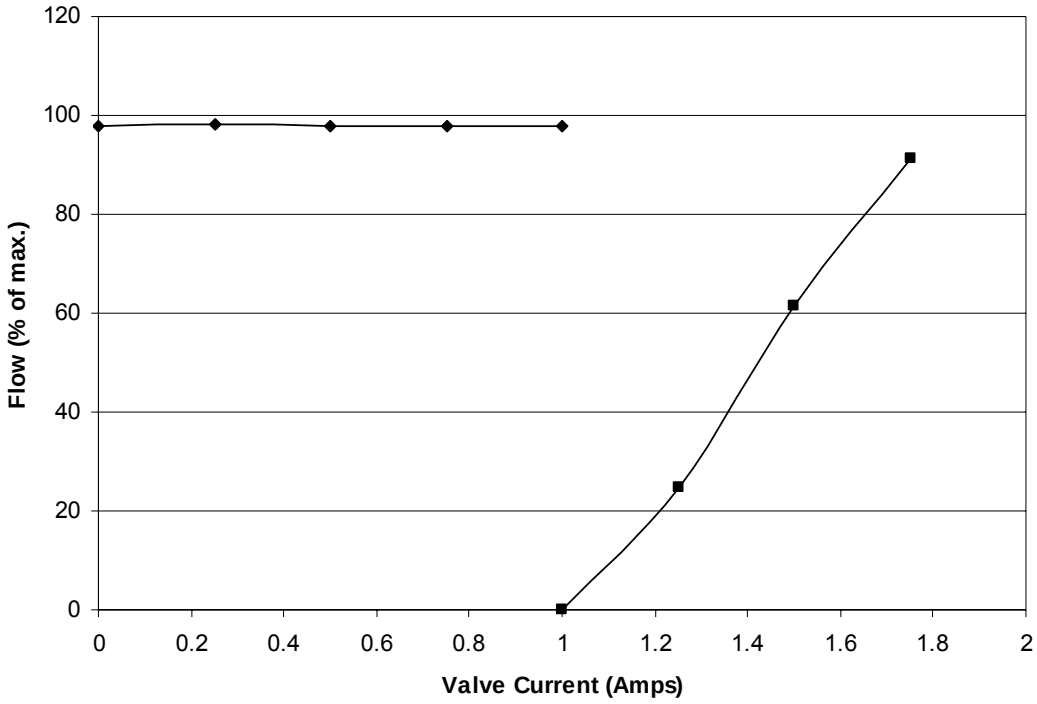

Figure 4. Erroneous data set acquired from manufacturer. Note that the flow data for the case of current less than 1 Amp is not valid

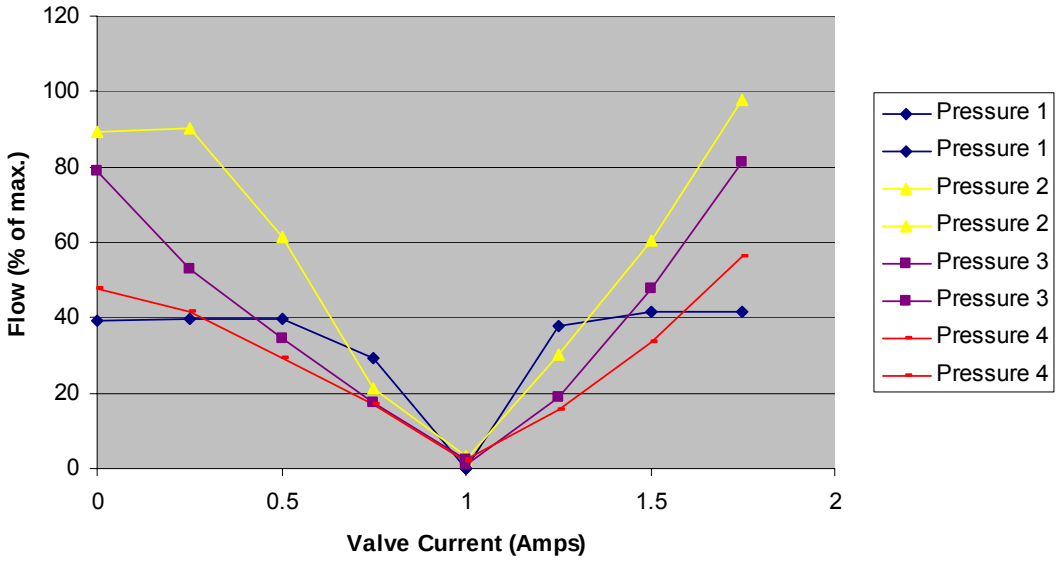

Figure 5. Complete set of flow data for several pressure drops across the valve.

The resolution to this issue was to mirror the available data sets to create new data sets. If information existed for flow through the failure port but not for port B, then the valve was assumed to be symmetrical and the available data was used to recreate the missing data. An example correcting the erroneous data shown in Figure 4 is shown in Figure 6. The justification for this action lies in the uncertainty analysis. The reason for using different control valves in this system is to study the uncertainty that is introduced when doing so (Chapter 3). If valve flow characteristics are assumed to be symmetrical through both ports, then the uncertainty due to this valve in the system is effectively zero. No variation in system performance can be observed when moving the valve's spool between the two outlet ports, therefore not affecting the system's uncertainty model. While this assumption might at first seem too liberal, it was the only option available considering the data supplied.

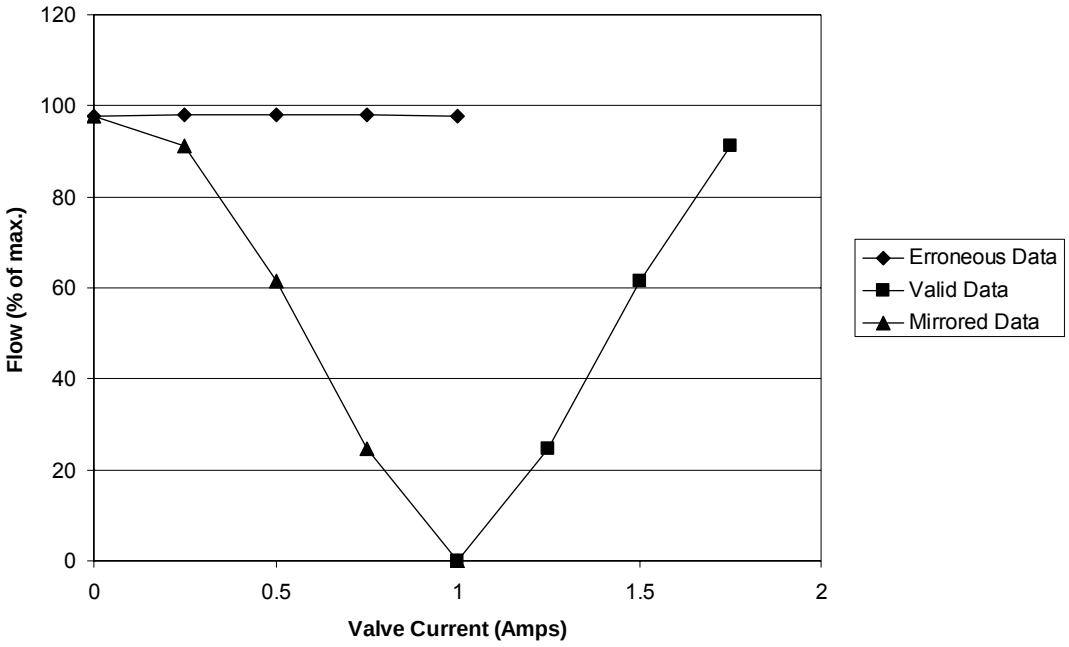

Figure 6. Example showing corrected flow data

It should be noted that the pressure that supplies the control valve has a lower limit. This limit is known as the charge pressure. A smaller pump runs alongside the larger hydraulic pump, supplying a constant pressure of 4.4 MPa. When the large pump's discharge pressure is lower than this value, a valve in the pump allows the charge pressure to supply the control valve. The reason for this action is that the pump must be primed before it can run normally. As the pump starts up, the pump pressure is 0 Pa (gage). To be able to increase the pump displacement, and therefore the pump pressure, the control cylinder must be moved. This cylinder can only be moved when a force imbalance exists between its two actuation areas (see Figure 2). If the pump pressure is not high enough to displace the control cylinder, then the pump pressure cannot, in turn, be increased. The charge pump solves this problem by supplying a constant pressure high enough for the initial displacement of the swash-plate when the pump pressure is too low to do so.

The control cylinder adjusts the position of the swash-plate mechanically. These two components are attached, and knowing the position of one equates to knowing the position of both. The control cylinder's actuation surfaces have two different areas, shown in Figure 2. The small area is acted upon by the pump pressure, while the large area is acted upon by the control pressure. While the control pressure tends to be lower than the pump pressure, the area difference between the two actuation surfaces allows for the movement of the cylinder in either direction. The sum of forces on the control cylinder can be written as

$$P_C A_C - P_P A_P = F_{SP} \tag{1}$$

where F_{SP} is the force exerted by the swash-plate on the control cylinder. The control pressure, P_C, is calculated using the pressure-rise rate equation

$$\dot{P}_C = \frac{\beta}{V}\left(Q - \dot{V}\right) \tag{2}$$

where β is the fluid bulk modulus, Q is the flow rate from the control valve into the control chamber, and V is the volume of the control chamber.

Once the force exerted on the swash plate by the control cylinder is calculated, the total torque on the swash plate can be found. Using all of the torque calculations thus far, the total swash plate torque is

$$\tau_{SP} = F_{SP} l_{SP} + \tau_{viscous} - \tau_{swivel} \tag{3}$$

where l_{SP} is the moment arm that the control cylinder acts upon, $\tau_{viscous}$ is the amount of torque due to viscous friction, and τ_{swivel} is the amount of torque due to flow forces. This moment arm is the distance between the control cylinder connection and the swivel point of the swash plate.

With the total torque on the swash plate calculated, the behavior of the swash plate can be analyzed. The rotational acceleration, $\ddot{\theta}$, of the swash plate is calculated using

$$\sum \tau = J_{SP}\, \ddot{\theta} = \tau_{SP}\,. \tag{4}$$

The rotational speed and position of the swash plate are then determined from this equation.

The position of the swash plate determines the displacement of the pump. When the swash plate's angle is at its maximum value, the pump is at full displacement. Likewise, when the swash plate's angle is zero, the pump is at zero

displacement. Also, in this pump the relationship between the swash plate angle and the pump's displacement is linear.

The next section modeled was the pump. The input to the pump is the flow rate from the displacement model. The output of the pump is the pump pressure.

The pump model consists mainly of unit conversions, efficiency calculations, and a single pressure-rise rate equation. The output of the displacement model is the volumetric displacement of the pump, in units of cm^3/revolution. In the pump model, the pump displacement is multiplied by the pump speed to obtain the ideal discharge flow rate of the pump. This value, though mathematically correct, is not the actual discharge flow rate of the pump. In practice, actual flow rate is less than the calculated theoretical value, due to the inherent inefficiencies within a hydraulic system. The actual discharge flow rate of the pump is a percentage of this ideal flow rate. This percentage is known as the "volumetric efficiency" of the pump.

The overall efficiency of a pump is equal to the product of its volumetric efficiency and its mechanical efficiency. The volumetric efficiency is calculated by

$$\eta_{vol} = \frac{Q_{observed}}{Q_{ideal}} \ , \tag{5}$$

while the mechanical efficiency is calculated by

$$\eta_{mech} = \frac{\tau_{observed}}{\tau_{ideal}} \ . \tag{6}$$

The model constructed for this study did not include an engine model, and therefore did not include values for engine torque. The engine was assumed to be ideal, running at a constant speed of 2000 rpm. The volumetric efficiency, however, was

used in this study. Volumetric efficiency data was provided by machine tests, using the calculation

$$Q_{ideal} = \frac{V_d}{\omega_{in}} \tag{7}$$

where V_d is the displacement of the pump and ω_{in} is the input speed to the pump.

The volumetric efficiency is a function of three variables: pump speed, pump displacement, and discharge pressure. In general, the volumetric efficiency increases as displacement increases and pump speed increases. The efficiency decreases as pump pressure increases.

With the correct pump flow calculated, the pump pressure can then be determined. The pressure rise rate equation from Eq. (2) is used to find the discharge pressure. The flow term used in this equation is shown to be

$$\sum Q = Q_{pump} - Q_{leak} - Q_{load} . \tag{8}$$

The flow rate loss due to leaks, Q_{leak}, is proportional to the pump pressure. This loss is equal to

$$Q_{leak} = K_l P_P \tag{9}$$

where K_l is the leak coefficient. For new hydraulic systems, this value is small and has little effect on the pressure rise rate equation. However, as a system ages, this leakage can become more of an issue and its effects can be felt through the entire system.

The flow rate through the load valve, Q_{load}, is also the flow rate passing through a downstream valve. The difference between the pump discharge flow rate and the load flow rate is equal to the flow rate entering the pump volume. For a low

flow rare passing through the downstream valve, this difference can be large, causing a large increase in pump pressure. If a high percentage of the discharge flow rate passes through the load valve, this difference shrinks and the pump pressure falls.

With the pump section completed and the pump pressure calculated, the final component is the downstream load valve. This valve consists solely of a flow restriction. Its input is the pump pressure and its output is the downstream flow rate. All of the flow passing through the load valve is returned to the hydraulic fluid storage tank.

The load valve model consists of a single equation: the orifice equation. This equation states that

$$Q = C_d A \sqrt{\frac{2}{\rho}(P_1 - P_2)} \ , \tag{10}$$

where the discharge coefficient, C_d, is set equal to 0.62 nominally. The fluid density, ρ, has a value of 850 kg/m^3, and the orifice's nominal area, A, is 0.50 cm^3. The inlet pressure of this valve is the pump pressure (noted as P_1), the outlet pressure is the atmospheric pressure (noted as P_2), and Q denotes the flow through the valve.

With all three components of the system modeled, some modeling strategies can be outlined. The most important issue in computer modeling of any system is accuracy. In a state-based model such as a hydraulic system, numerical accuracy issues may arise from the integration routines used to solve the system's governing differential equations. Since the integration used in numerical solvers is generally geometrical, the size and scale of the integrated values, relative to one another, is important. For simplicity's sake, the numerical simulation tool used in this project (Simulink) requests an overall accuracy requirement spanning the entire model.

Because this requirement is a scalar and not a percentage, it is not possible to demand the same accuracy of two separate integrators if one calculates a pressure state in units of Pascals (generally on the scale of 10^6) and another calculates a radial position state in units of radians (on a scale of 0-3). If the accuracy required of the position state were converted to the pressure state, the simulation speed would slow to an unusable speed.

To combat this effect, the pressure integrators in the system were scaled. The integrators in the system that calculated the control chamber pressure and the discharge pressure were scaled by a factor of one million. For example, these integrators would now calculate a pressure state that varied between 0.1 and 10, whereas before they calculated states varying between 100,000 and 10,000,000. The accuracy required for this integration routine would then be equivalent to the accuracy required of the position states mentioned earlier.

To summarize the first-principles model, the four equations of the system are presented in Eqs. (11 – 14). Expressing the state derivative equations in this manner will also aid in organizing the linearization section in this chapter.

$$\dot{x}_1 = \dot{P}_C = \frac{\beta}{V_{control}}\left(Q - \dot{V}_{control}\right) \tag{11}$$

$$\dot{x}_2 = \dot{P}_P = \frac{\beta}{V_{pump}}\left(Q_{discharge} - \dot{V}_{pump}\right) \tag{12}$$

$$\dot{x}_3 = \ddot{\theta} = \frac{\sum \tau_{SP}}{J_{SP}} \tag{13}$$

$$\dot{x}_4 = \dot{\theta} = x_3 \tag{14}$$

2.2 Model Validation Using Test Data

The design model includes certain assumptions and approximations. These were necessary for model completeness, and also to ensure that the system was simple enough to analyze using the resources available. The most notable assumption made was that the control valve dynamics were not necessary to model; the undamped natural frequency of the control valve was estimated to be

$$\omega_n = \sqrt{\frac{k}{m}} \approx 300 \ rad/s \approx 50 \ Hz \tag{15}$$

where k is the valve spring constant and m is the mass of the spool. The speed of response of this valve is assumed to be fast enough so as not to impact the model.

The justification for the assumptions and approximations made in this study lies in the requirements for robustness. The control scheme that will eventually be designed for this system will emphasize robustness to system variance and disturbances. These modeling assumptions can be treated as system variances in that respect.

The nonlinear system model of the pump was compared with the machine test data in terms of displacement. The test data provided gives the volumetric displacement of the model as a function of time. The input to the machine is the current supplied to the control valve within the pump which, in turn, adjusts the swash-plate angle. The current profile is a pulse input, varying the pump displacement from minimum to a preset value. The current data provided was used as the input to the nonlinear model, and the displacement of the pump was compared with the machine test data under four different circumstances: 25% displacement, 50% displacement, 75% displacement, and 100% displacement. Plots of the

comparisons of the swash plate angle response between test data and nonlinear simulations can be found in Figures 7-10.

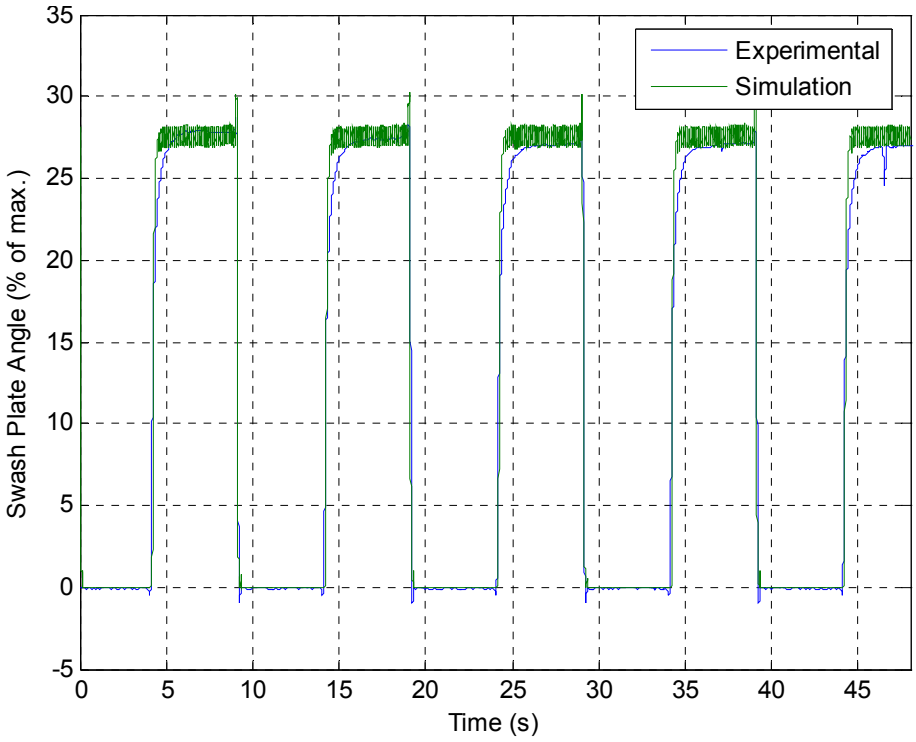

Figure 7. Comparison of nonlinear simulation and machine test data. The displacement here pulses between minimum displacement and 25% displacement.

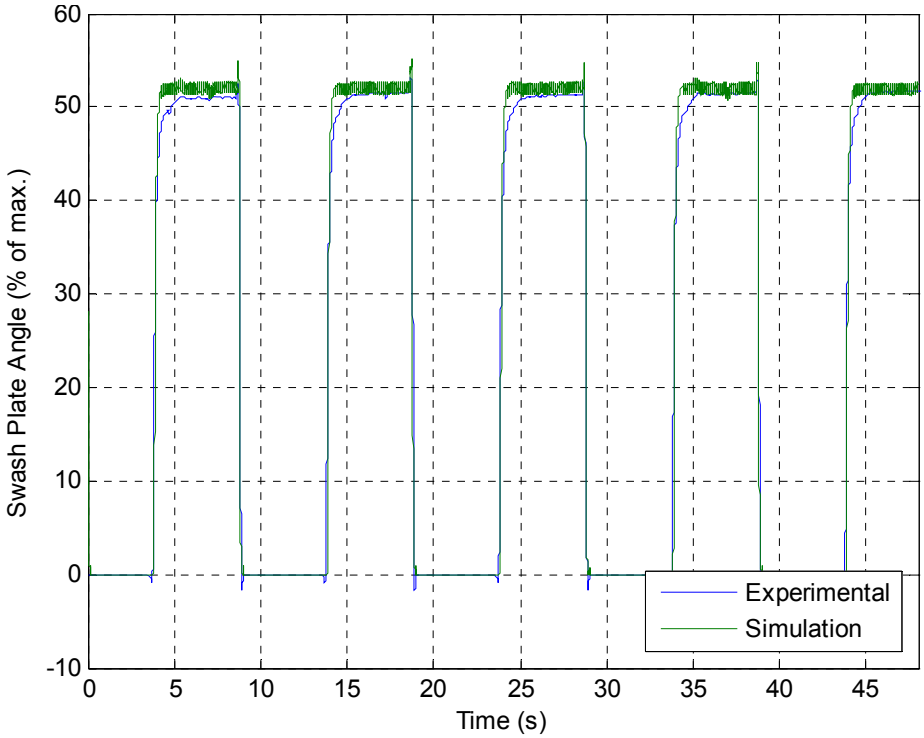

Figure 8. Comparison of nonlinear simulation and machine test data. The displacement here pulses between minimum displacement and 50% displacement.

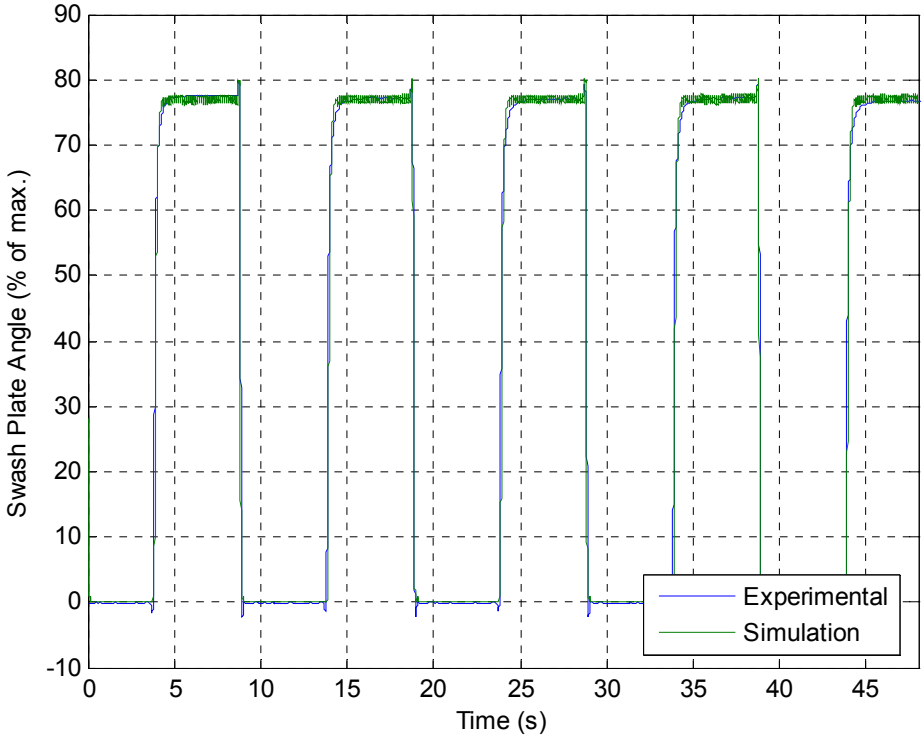

Figure 9. Comparison of nonlinear simulation and machine test data. The displacement here pulses between minimum displacement and 75% displacement.

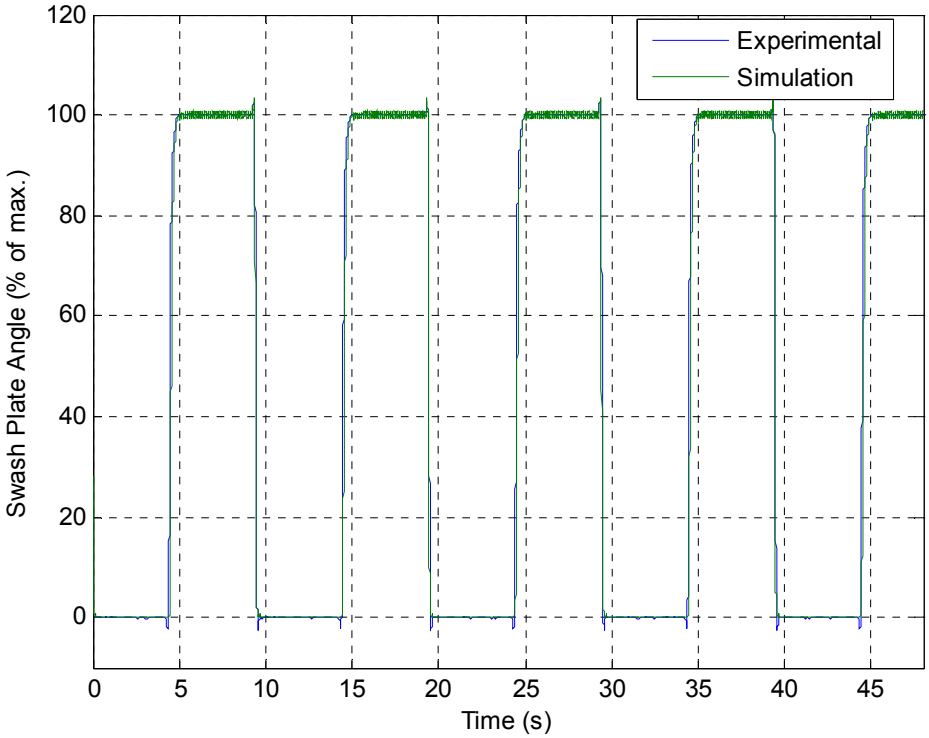

Figure 10. Comparison of nonlinear simulation and machine test data. The displacement here pulses between minimum displacement and 100% displacement.

From these comparisons it is apparent that the nonlinear pump model matches up well with the real model. The variations observed in Figures 7 and 8 can be attributed to the fact that a mechanical efficiency model was not included in the system, since most of the variation disappears as the displacement increases. Mechanical efficiency, like volumetric efficiency, increases as displacement increases.

The errors observed here are within the boundary of being acceptable. The inaccuracies shown can be included in future control design, since the goal of robust control design is to account for system variation. Some of the discrepancies between the nonlinear model and the machine test data will also be addressed in the uncertainty analysis in this chapter.

2.3 Model Linearization

While the nonlinear model of the system has proved to be accurate, in its current state it is difficult to study. This is because most control techniques require a linear system model, preferably in a state-space format.

Linearization of a system is generally done by analyzing the state equations and constructing first-order Taylor series expansions of them. The pump model makes this technique nearly impossible. The presence of nonlinearities such as the look-up tables for calculating swivel torque, control valve flow, and volumetric efficiency makes studying the system equations less useful. Instead of mathematically linearizing the system from its constituent state equations, a numerical technique was used. Using the numerical solver software package *Matlab* and numerical simulation program *Simulink*, a linear model could be found. The *Matlab* utility "linmod.m" uses a finite-differencing linearization method to construct a state-space model of a nonlinear system.

Finite-differencing is a numerical method for building the system matrices of a model. By perturbing each state incrementally and then observing the state derivative vector response, the system matrices can, in turn, be constructed. By using the approximation

$$\frac{\partial f_n}{\partial x_m} \approx \frac{\Delta f_n}{\Delta x_m} = \frac{f_{n,nom} - f_{n,perturb\,xm}}{x_{m,nom} - x_{m,perturbed}} \tag{16}$$

each individual element of the A and B matrices can be found, where f_n is the nth state derivative function. The system matrices can be calculated by using

$$A = \begin{bmatrix} \frac{\partial f_1}{\partial x_1} & \frac{\partial f_1}{\partial x_2} & \cdots \\ \frac{\partial f_2}{\partial x_1} & \frac{\partial f_2}{\partial x_2} & \\ \vdots & & \ddots \\ & & \end{bmatrix} \tag{17}$$

and

$$B = \begin{bmatrix} \frac{\partial f_1}{\partial u_1} & \frac{\partial f_1}{\partial u_2} & \cdots \\ \frac{\partial f_2}{\partial u_1} & \frac{\partial f_2}{\partial u_2} & \\ \vdots & & \ddots \\ & & \end{bmatrix}. \tag{18}$$

Upon creating the linearized system, verification was necessary to ensure that the future analysis would be valid. The states of the linear model needed to be compared with those of the nonlinear model. A small disturbance of 0.1% was given to both models via the current input, and the responses of the four states of the system to this disturbance are compared in Figure 11 through Figure 14. The nominal operating point in this test is

$$\vec{x}_0 = \begin{bmatrix} P_C \\ P_P \\ \dot{\theta} \\ \theta \end{bmatrix} = \begin{bmatrix} 0.206\ MPa \\ 0.622\ MPa \\ 0\ rad/s \\ 0.048\ rad \end{bmatrix}. \tag{19}$$

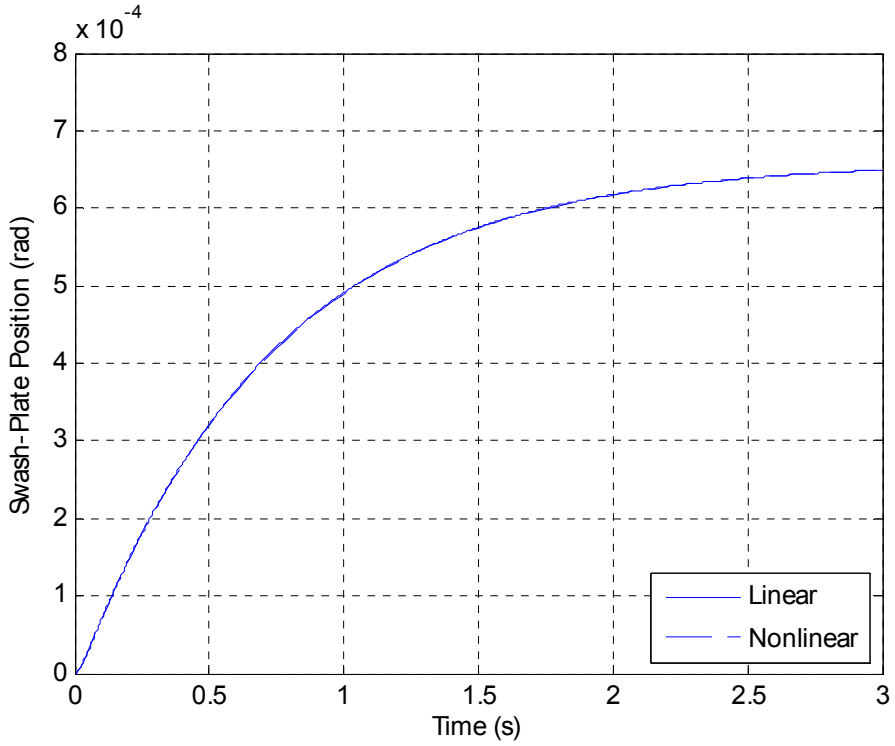

Figure 11. Comparison of the swash-plate position state between the linear and nonlinear models.

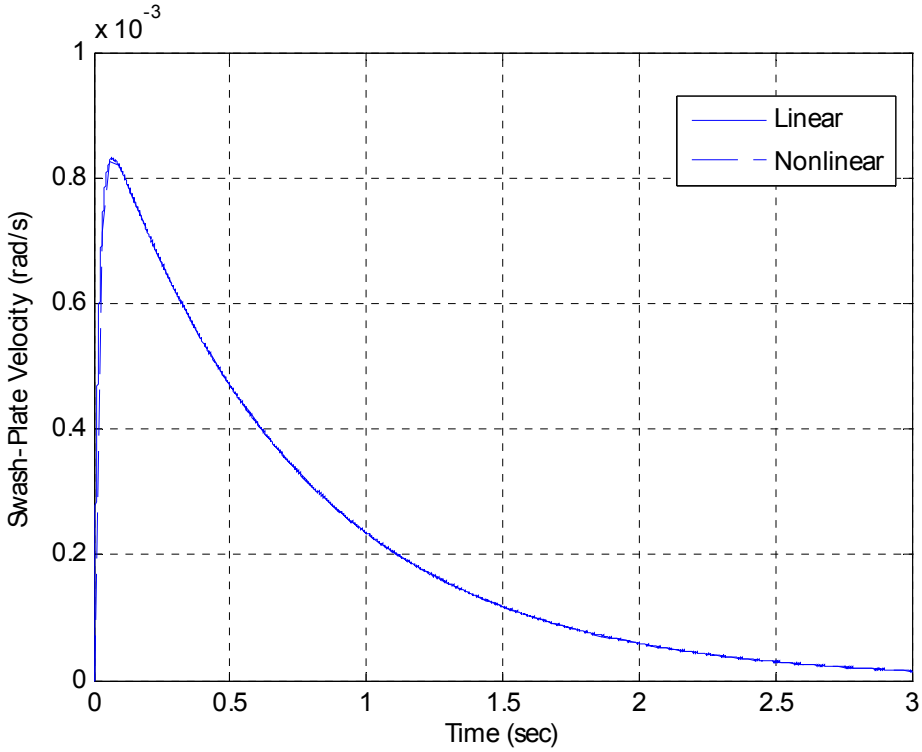

Figure 12. Comparison of the swash-plate velocity state between the linear and nonlinear models.

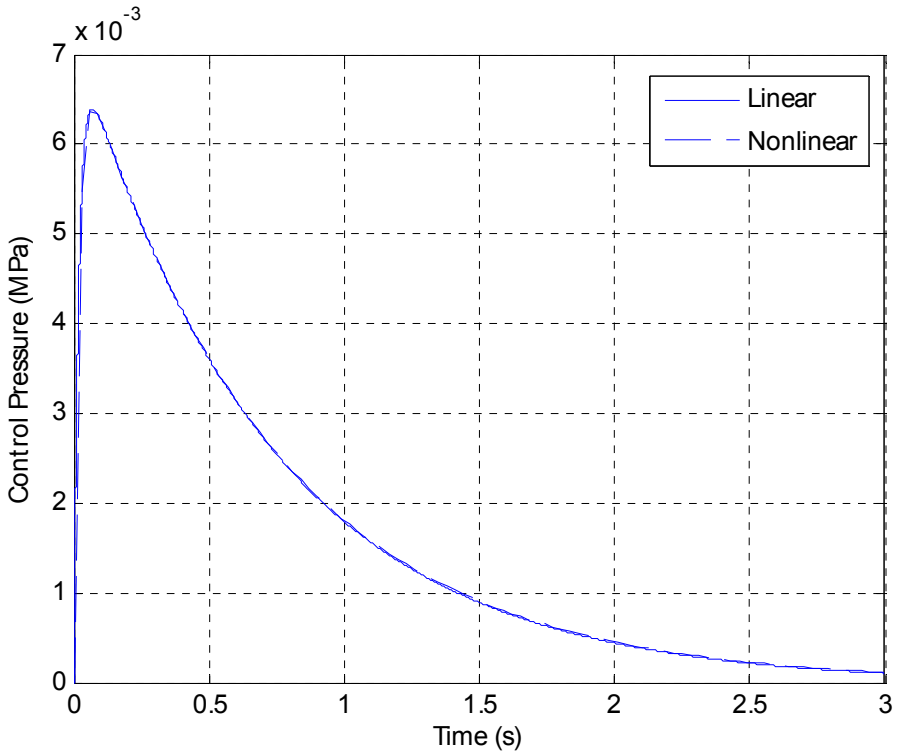

Figure 13. Comparison of the control pressure state between the linear and nonlinear models.

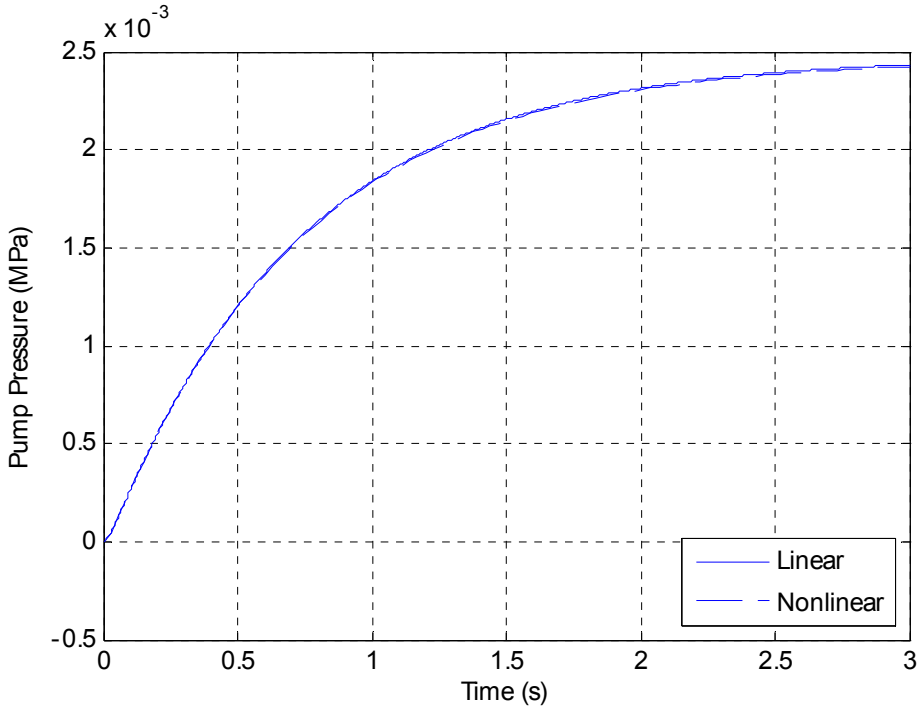

Figure 14. Comparison of the pump pressure state between the linear and nonlinear models.

The two systems exhibit similar responses to the step disturbance inputs with comparable dynamics as shown. The linearization is accurate enough so that the linear and nonlinear state responses lie on top of one another in the comparison plots.

Due to the fact that the linearized system was built from knowledge of the non-linear system, the same limitations that applied to the original full-state simulated model apply to the linearized approximation of it. The only addition to those limitations is the fact that linearized systems tend to be less accurate as the system deviates from the point of linearization. Again, these discrepancies will be accounted for in the robustness analysis and will not cause any significant future problems.

Once the linear model of the system has been created, linear analysis can be applied. One of the most powerful tools in linear system analysis is the pole-zero map of a system. This plot can, at a glance, show a significant amount of information about a system including stability, performance limitations, and response characteristics. The pole-zero map of the linear pump model is shown in Figure 15

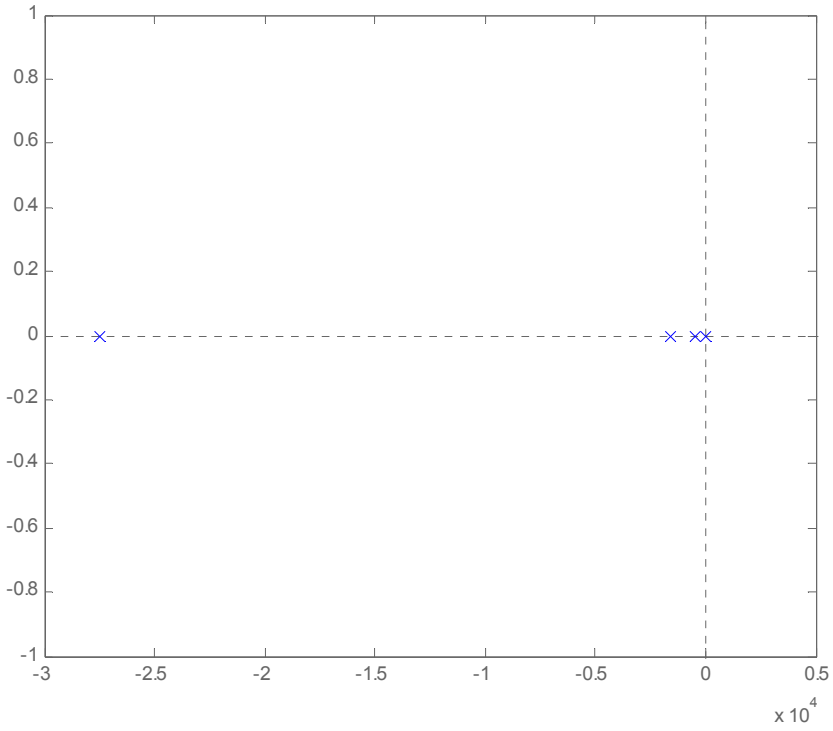

Figure 15. Pole-zero map of the linear system.

All of the poles of the system lie in the left-half s-plane, implying that the system is asymptotically stable. The single pole that lies far away from the other three implies that one of the states of the system will react much faster than the others. Also, there are no zeros that lie in the right-half s-plane, meaning that there are no inherent performance limitations observed.

One important finding from studying the pole-zero map is that one of the assumptions made about the system may be incorrect. Earlier, it was hypothesized that the dynamics of the control valve were fast enough to neglect modeling. However, it would seem from observing the pole-zero map in Figure 15, that the dynamics of the valve, calculated from Eq. (15), are necessary to study. The three poles of the system nearest the origin lie between R= 0 rad/sec and R= -1600 rad/sec.,

resulting in a dynamic system with a natural frequency of oscillation of about 300 rad/sec, which is significant for study. In this case, the dynamics of the control valve may interact with the dynamics of the previously modeled system, resulting in unexpected effects.

However, rebuilding the first principles model of the system is not necessary, even after this late discovery. To simulate the dynamics of the control valve, a second-order transfer function of the form

$$F(s) = \frac{\frac{k}{m}}{s^2 + \frac{b}{m}s + \frac{k}{m}} \tag{20}$$

is cascaded with the electric current input to the system, representing the effect of a mass-spring-damper system. In Eq. (20), the spool damping is shown as b. The valve is assumed to have a maximum overshoot of 5%, resulting in a damping term of $b = 0.707$. This assumption is necessary because no damping information for this particular spool valve is available. This transfer function has a unity dc-gain, meaning that it can be added to the system in series, as shown in Figure 16. Because transfer functions are so well understood, no analysis of the simulated spool valve dynamics and their effect on the linear model is needed. However, it should be noted that the addition of the transfer function in Eq. (20) increases the number of states in the system from four to six.

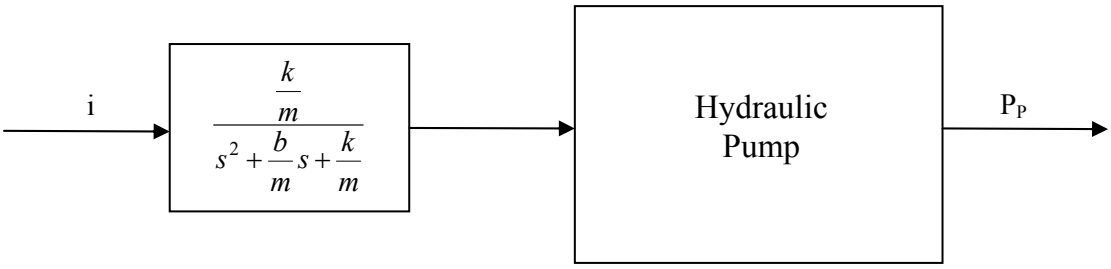

Figure 16. Block diagram of system with spool valve dynamics simulated by transfer function

Chapter 3

UNCERTAINTY MODEL

3.1 Defining System Uncertainty

In a robustness study, it is important to determine the amount of variance that exists within a system. A robust controller is designed such that it can maintain stability under all expected operating conditions, making it important to establish what these conditions might be. By creating an uncertainty model, the variance within a system can be quantified. The uncertainty model will be used in ensuing chapters to calculate the level of robustness of a controlled system.

An uncertainty model is, essentially, a statement of the maximum variance the system will experience, making it a "worst-case scenario". Mathematically, an uncertainty model is a transfer function that represents the maximum error in the output of a system. A block diagram showing the architecture of a system with a multiplicative output uncertainty model (w_O) is shown in Figure 17.

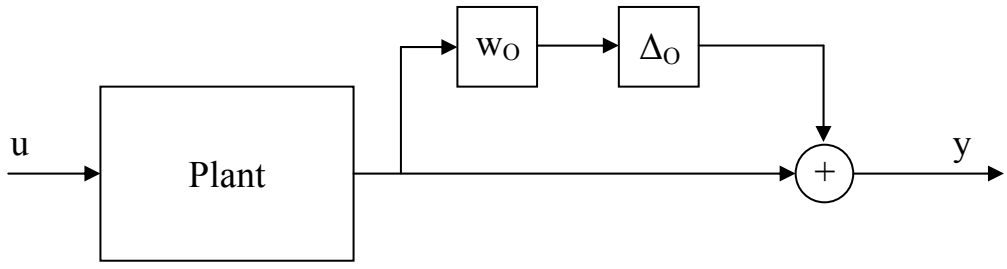

Figure 17. Block diagram displaying system uncertainty

The as-yet unexplained parameter shown in Figure 17 is the complex perturbation matrix Δ. This accompanying term is the set of all transfer function matrices whose maximum singular value is less than one. The Δ term can be thought

of as a scaling matrix: essentially a gain within the system that will amplify its input to a value between ±100% of the input (±1) over all frequencies. This term is, in practice, ignored and is generally only addressed in mathematical derivations in robust control analysis. The focus of this project will remain on the output uncertainty, w_O.

There are many different configurations for analyzing uncertainty. The multiplicative output uncertainty design shown in Figure 17 is one choice. The choice of which uncertainty configuration to use is left to the analyst. Some of the other uncertainty configuration choices are input multiplicative uncertainty (Figure 18-a), inverse multiplicative input uncertainty (Figure 18-b), and inverse multiplicative output uncertainty (Figure 18-c). For this project, the multiplicative output uncertainty configuration was chosen over the others for several reasons. For a single-input single-output (SISO) system, there is no difference between the calculation of input multiplicative uncertainty and output multiplicative uncertainty, which will be shown. Also, the multiplicative uncertainty configuration was chosen over the inverse multiplicative uncertainty configuration because of the nature of the system. In this model, parameter fluctuations and operating point variation are expected to have an effect similar to a steady-state error in the output. Inverse multiplicative uncertainty, conversely, would cause an increasing error in the output as time passed.

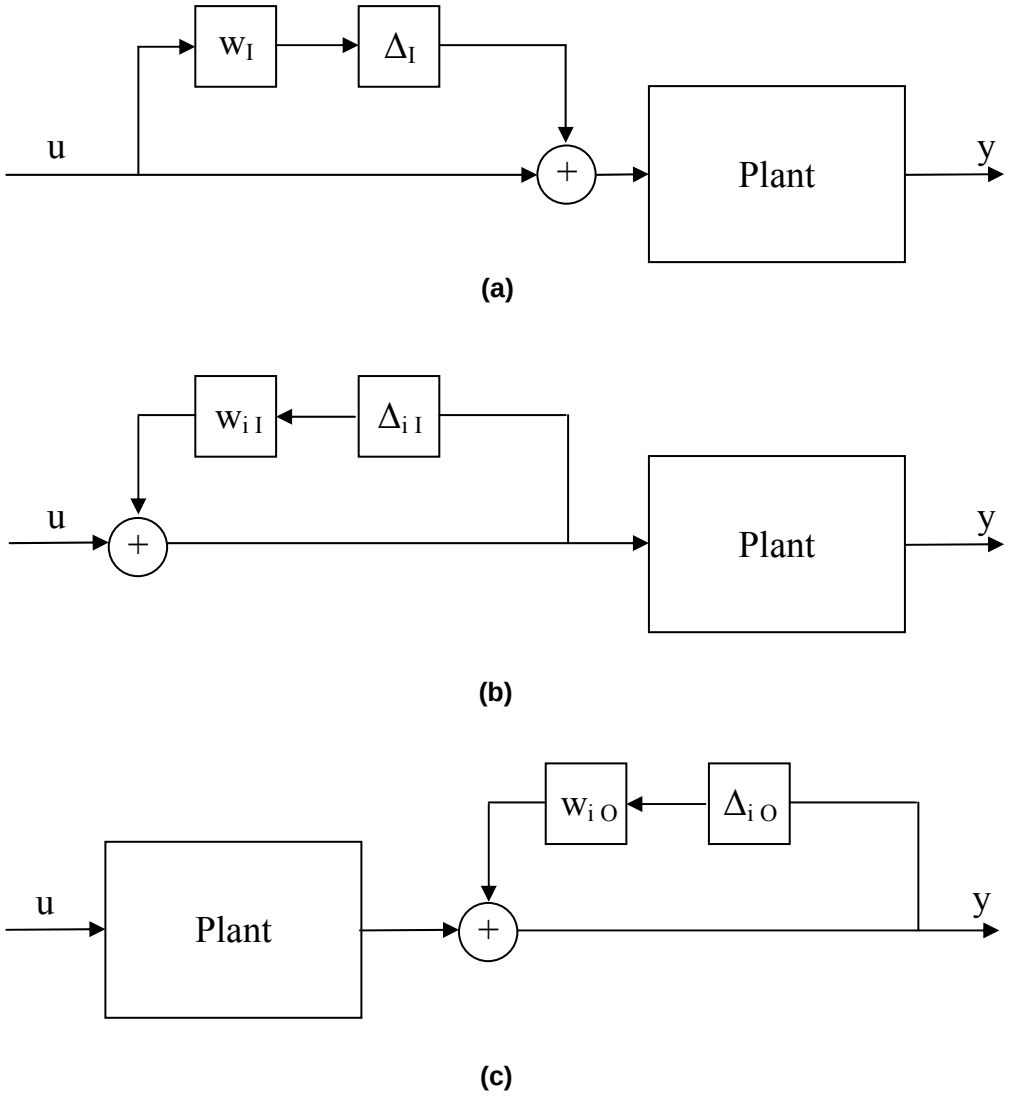

Figure 18. (a) Multiplicative input uncertainty, (b) Inverse multiplicative input uncertainty, (c) Inverse multiplicative output uncertainty.

It is important to realize that the uncertainty in a system is equivalent to its variation from a nominal case. The uncertainty model of a system attempts to incorporate the complete range of variance of that system. Therefore, it should be noted that one of the goals of uncertainty analysis is to achieve the least conservative uncertainty description possible that retains accuracy. This is important in order to

prevent overestimates of uncertainty in the robustness analysis (Chapter 3), creating a controller that is too conservative.

With an uncertainty architecture selected, calculation of the uncertainty transfer function w_O can begin. The first step in this process is to determine which properties of the system will vary. It was determined in [8] that the uncertainty within a hydraulic system increases as the system strays from its nominal operating point. Therefore, one of the main variances in this study will be the system's integrity as it drifts from this point. Another concern within a hydraulic system is the fluctuation of fluid parameters. The fluid bulk modulus (β) can vary due to many different operating situations [8], [9] and will be included in this uncertainty study.

Another cause of uncertainty within a system is manufacturing variability. Tolerances and errors of a machined part can significantly impact a system's characteristics. In this model, the control valve within the pump is subject to this variability. Several different manufacturers each provided several separate spool valves to be used in this study. Each valve's flow coefficient is different, varying from an average value by some percent. As this deviation from the average increases, the uncertainty due to using the corresponding valve also increases.

The final source of uncertainty explored is that due to different pump applications. The pump studied in this project will be used for many different functions, and therefore, the load valve as modeled earlier will change for each application. In other words, a constant load valve area is not realistic since load valves generally control flow to hydraulic implements. A load valve's area changes as the requirements of the load change.

To calculate the uncertainty of a system, the set of perturbed plants must first be defined. The set of perturbed plants (G_p) is the collection of all possible linear plants given every combination of uncertain characteristics. Its variance from the nominal plant is normalized by calculating

$$w_O \Delta_O = \left[\left(G_p(j\omega) - G_{nom}(j\omega) \right) G_{nom}^{-1}(j\omega) \right]. \tag{21}$$

Using the property that

$$\max\left(\Delta_O(j\omega) \right) = 1 \ \ \forall \omega, \tag{22}$$

one can calculate the uncertainty description outright:

$$w_o \geq \max_{G \in \Pi} \left[\left(G_p(j\omega) - G_{nom}(j\omega) \right) G_{nom}^{-1}(j\omega) \right] = \max_{G \in \Pi} \left(l_O \right) \tag{23}$$

The uncertainty description calculated in Eq. (23) is known as the "lumped uncertainty" model. By calculating w_O in this manner, the assumption is made that every uncertain parameter in the model affects the output of the model in the same manner. This is equivalent to declaring an entire machine as "broken" when, in reality, only a small piece or several small pieces of it are in need of repair. The alternative to lumped uncertainty, known as structured uncertainty, will be presented later in this chapter. However, a lumped uncertainty model can be very accurate for simple systems and is an excellent starting point for an analysis.

3.2 The Lumped Uncertainty Model

The varying conditions within the model should be outlined first. The two varying physical conditions within the system (fluid bulk modulus and load valve

area) were each allowed to vary over a range of possible values centered around a nominal value. The full range of variance for each parameter is outlined in Table 1.

Table 1. Parameter variation within the hydraulic system

Parameter	Lowest Value	Nominal Value	Highest Value
Bulk Modulus, β	1.050 GPa	1.575 GPa	2.010 GPa
Valve Area	0.10 cm^2	0.30 cm^2	0.50 cm^2

The variance within the system due to a changing operating point can best be summarized by outlining the operating points explored in the analysis. Table 2 contains information on the four separate states of the system at the six operating points investigated. Notice that the fourth operating point investigated is the nominal operating condition. The operating point of the system is allowed to vary by adjusting the input to the system and linearizing the system using the new input.

Table 2. The six operating points studied in uncertainty analysis.

Operating Point	Pump Pressure (MPa)	Control Pressure (MPa)	Swash-Plate Position (rad)	Swash-Plate Velocity (rad/s)
1	5.98	3.86	0.150	0.156
2	5.01	3.03	0.137	0.104
3	3.78	2.39	0.119	0.057
4 (nom)	2.69	1.96	0.100	0.000
5	1.49	1.46	0.075	-0.064
6	0.93	1.18	0.059	-0.101

The 13 separate control valves used in the uncertainty analysis were each treated as a variation from a nominal valve. The nominal valve characteristics were calculated by creating an "average valve." This average valve consisted of a look-up table that calculated flow for a given set of pressure and input current conditions, in a manner similar to each of the other 13 valves. Each value contained within the average valve's look-up table was the average value calculated from all 13 valves at that operating condition.

A perturbed plant, G_p, can be constructed with a specific knowledge of the varying parameters and conditions. First, however, each plant must be scaled to allow for analysis on an relative scale. To scale a plant, the maximum expected input (u_{max}) and output (y_{max}) must first be defined. The plant, G, must then be arranged as shown in Figure 19 to find G_{scaled}.

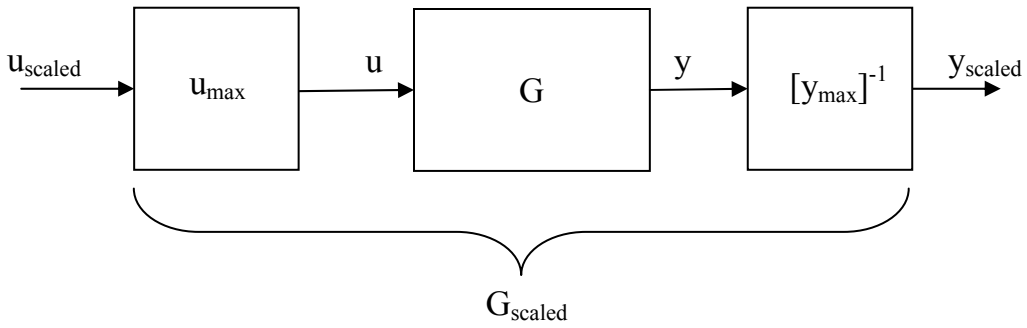

Figure 19. Example of plant scaling.

After exploring every possible combination of plant variances, the frequency responses of the normalized, varied systems are plotted in Figure 20. This is equivalent to a plot of Eq. (21) for the pump model *G*.

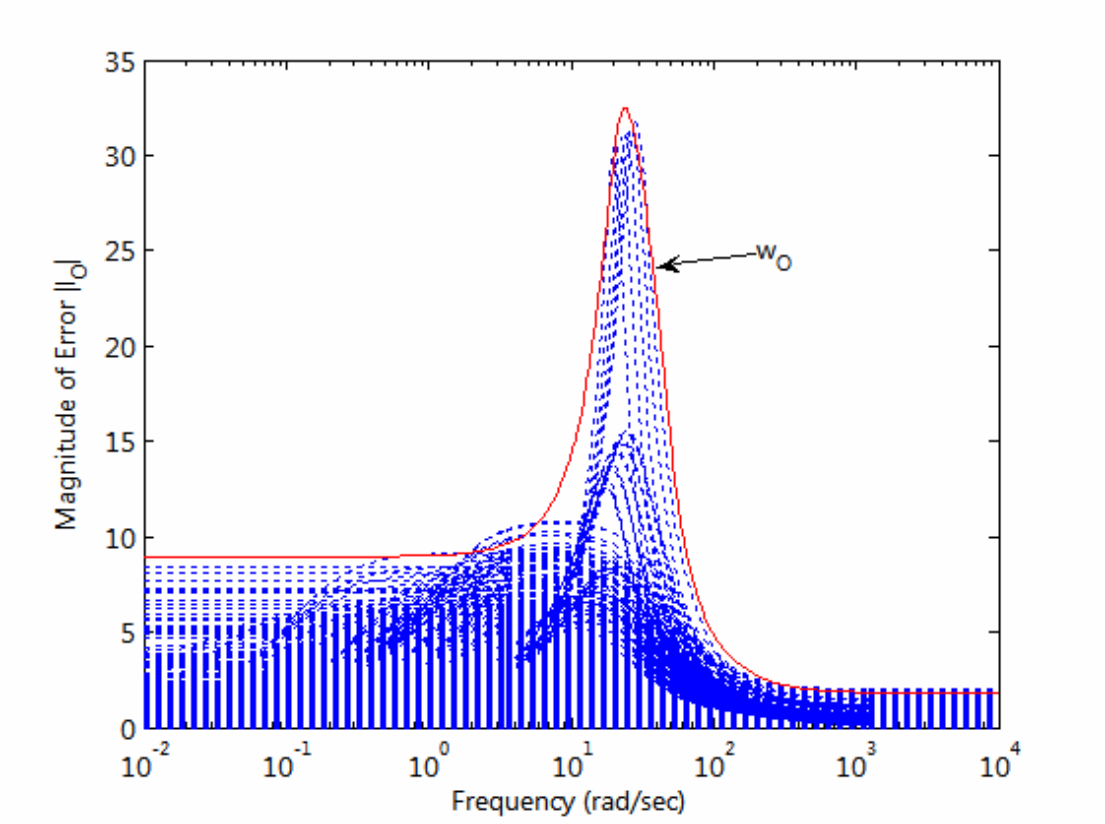

Figure 20. Output uncertainty transfer function

In Figure 20, the perturbed plant errors, l_O, are shown as dotted lines while the solid line represents the bounding transfer function, w_O. This transfer function represents the worst possible plant variation under the given conditions. The scale of Figure 20 is absolute, meaning that the system error at low frequencies is equal to 800% while the maximum error is over 3000%. The significance of these values is that the plant output is expected to vary, under worst-case conditions, between 800 and 3000% over the operating frequencies of the pump. This amount of variance seems unusually high, and in reality it is unlikely that the system could vary by such a large amount. The lumped uncertainty model does not appear to provide the accuracy required for this application. A robustly stable control design would be difficult to achieve with such a large uncertainty.

3.3 The Structured Uncertainty Model

The second, more precise, approach to modeling system uncertainty is structured uncertainty. In the structured uncertainty approach, each component of the model is analyzed as an individual plant. The uncertainty for each component is determined, yielding a much more accurate and less conservative system uncertainty model.

The pump model was separated into the following components for structured uncertainty analysis: the displacement model and the pump/load model. The displacement model consists of the architecture of the same name as described in Section 2.1, while the pump/load model is a combination of the pump model and the load valve model as described in the same section. The two inputs of the

displacement model are the valve current and the pump pressure, while its output is the pump discharge flow rate. The input to the pump/load model is the pump discharge flow and its output is the pump pressure. Performing individual uncertainty analyses on these two components results in the block diagram structure shown in Figure 21.

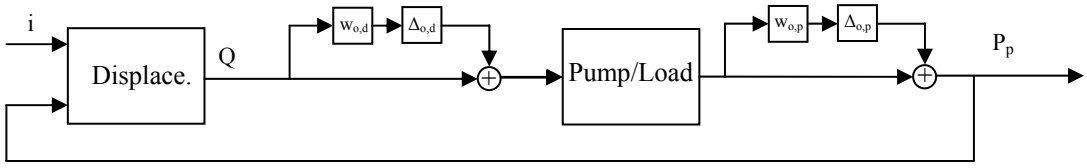

Figure 21. Block diagram of structured uncertainty architecture

The calculation of the uncertainty description w_O for each component is identical to the uncertainty calculation described by Eq. (14). The only observation here is that the order of matrix multiplication must be preserved when calculating the uncertainty of the displacement model. The displacement model is a Multiple-Input Single-Output (MISO) system, meaning that simple magnitude plots of its frequency response are not sufficient to describe its behavior. The analogy of the magnitude plot of a SISO system in the MISO and MIMO (Multiple-Input Multiple-Output) domains is the singular value function, σ. The singular value of a plant G is defined as

$$\sigma(G) = \left[\frac{\|Gu\|_2}{\|u\|_2} \right], \tag{24}$$

where u is the input vector. The 2-norm of a vector ($\|\cdot\|_2$) is defined as

$$\|\vec{x}\|_2 = \sqrt{\sum x_i^{\,2}} \ . \tag{25}$$

The singular value of a system can be thought of as the gain of the system from its inputs to its outputs. The maximum singular value of a system at a frequency is the maximum gain of the system from its inputs to its outputs at that frequency. Therefore, to calculate the uncertainty of a MISO system, w_O must be found by

$$w_o = \max_{G \in \Pi} \bar{\sigma} \left[\left(G_p(j\omega) - G_{nom}(j\omega) \right) G_{nom}^{-1}(j\omega) \right] \tag{26}$$

where $\bar{\sigma}$ is the maximum singular value of a system at a given frequency.

By using structured uncertainty, the number of varying parameters within a component is less than the total number of varying parameters. For example, because the control valve chosen in the displacement model has no impact on the pump/load model, this component does not need to be varied when looking at the uncertainty description of the pump/load model. When analyzing the displacement model, the operating point, fluid bulk modulus, and control valve chosen were allowed to vary. When analyzing the pump/load model, the operating point, fluid bulk modulus, and load valve area were allowed to vary. The uncertainty description for the displacement model, $w_{O,d}$, is shown in Figure 22.

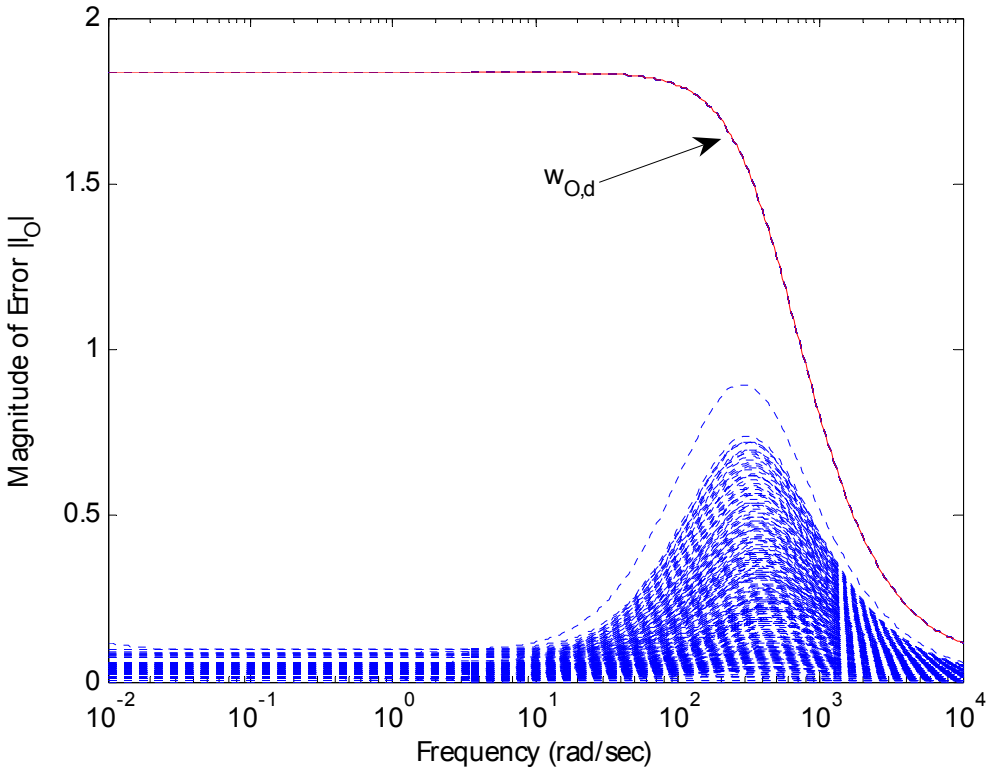

Figure 22. Uncertainty description of the displacement model.

The uncertainty description shown in Figure 22 does not appear to be accurate. Two outlying uncertainty cases exist, one with a low frequency error of nearly 200% and another with an error near 80%. The root of this problem was the inclusion of two specific valves in the uncertainty study. The presence of these two valves increased the uncertainty of the system dramatically, and they were therefore removed from the study as outliers. The revised uncertainty description $w_{O,d}$ is shown in Figure 23, while the uncertainty description of the load valve model, $w_{O,p}$, is shown in Figure 24.

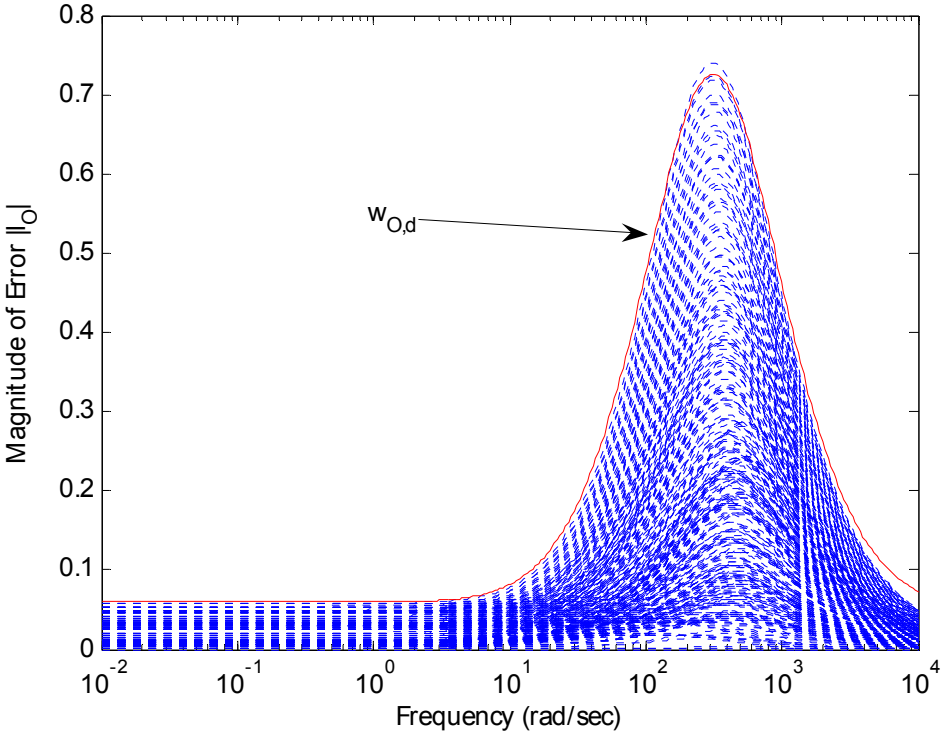

Figure 23. Uncertainty description of the displacement model

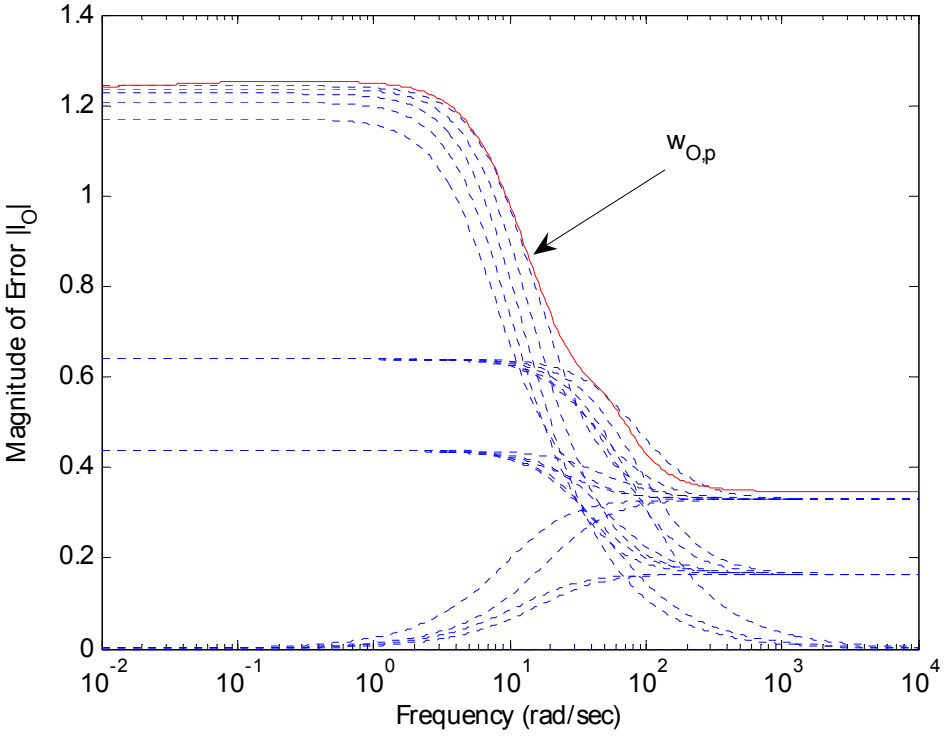

Figure 24. Uncertainty description of the pump/load model.

The results seen in Figure 23 and Figure 24 are encouraging. The uncertainty observed in the displacement model is equal to 6% at low frequencies and increases to 74% at a frequency of 316 rad/s (50.4 Hz). The uncertainty seen in the pump/load model is equal to 125% at low frequencies decreasing to a high-frequency uncertainty of 32%. While uncertainties of this magnitude might seem rather high, they are actually manageable in the field of robust control design and far better than the result for the lumped uncertainty case.

Chapter 4

H_∞ CONTROL DESIGN

4.1 The Case for H_∞ Control

H_∞ control methods were developed in response to the poor robustness qualities of LQG control, outlined in [7], [9]. The earliest use of H_∞ optimization techniques is found in the work by Helton in 1976, however, the majority of development in the field occurred in the 1980s. Research by Zames, Helton, Glover, and Doyle sought to develop the control design methods known as H_∞ and H_2. These methods were modeled to both achieve robustness properties not possible with LQG control, and also introduce a more realistic disturbance model than previously available [7]. The following sections establish a general control problem formulation, applicable to all H_∞ problems of interest, and a design algorithm for a specific H_∞ control design.

4.2 The Generalized Plant

While the approaches of H_2 and H_∞ are both reasonable with regard to modern control design, only the optimizations associated with H_∞ will be pursued in this study. The reasoning behind this decision lies in the similarity between the two methods. Both H_2 and H_∞ require the solutions to Riccati equations. Both yield controllers of state-dimension equivalent to that of the generalized plant *P*. Finally, both exhibit a controller/observer separation structure in the controller architecture already seen in LQG control [7].

The design of H_∞ controllers differs from application to application, making it useful to have a standard problem formulation in which any specific control problem can be expressed. This general formulation is described by

$$\begin{bmatrix} z \\ v \end{bmatrix} = P(s)\begin{bmatrix} w \\ u \end{bmatrix} = \begin{bmatrix} P_{11}(s) & P_{12}(s) \\ P_{21}(s) & P_{22}(s) \end{bmatrix}\begin{bmatrix} w \\ u \end{bmatrix}, \tag{27}$$

$$u = K(s)v \tag{28}$$

with a state-space representation of the generalized plant, P, expressed by

$$P \overset{s}{=} \begin{bmatrix} A & B_1 & B_2 \\ C_1 & D_{11} & D_{12} \\ C_2 & D_{21} & D_{22} \end{bmatrix}, \tag{29}$$

where the u represents the control variables, w represents the exogeneous signals (such as noise), z represents the error signal, and v represents the measured variables. This generalized plant is shown in Figure 25.

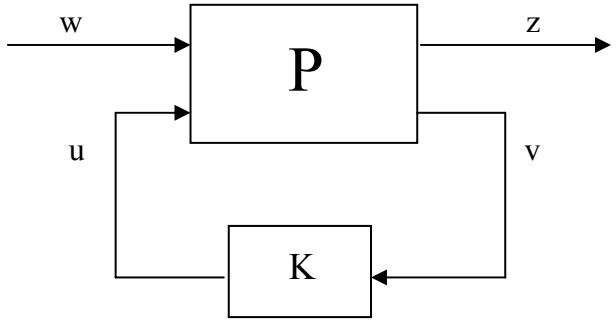

Figure 25. General control configuration

Skogestad et al. [7] shows that the transfer function matrix from input w to error signal z can be expressed by the linear fractional transformation

$$z = F_l(P, K)w \tag{30}$$

where

$$F_l(P,K) = P_{11} + P_{12}K(I - P_{22}K)^{-1}P_{21}. \tag{31}$$

Note that in Eq. (31), the notation P_{ij} represents the transfer function from the *i*th input to the *j*th output. Using Eq. (32), the H_∞ optimal control problem is to find all stabilizing controllers *K* which minimize the infinity norm

$$\left\|F_l(P,K)\right\|_\infty = \max_\omega \bar{\sigma}(F_l(P,K)(j\omega)), \tag{32}$$

where the infinity (∞) norm is calculated by

$$\left\|F_l(P,K)\right\|_\infty = \max_{\omega(t)\neq 0} \frac{\left\|z(t)\right\|_2}{\left\|w(t)\right\|_2}. \tag{33}$$

The 2-norm of a vector is described in Eq. (25).

Skogestad et al. states that, "In practice, it is usually not necessary to obtain an optimal controller for the H_∞ problem, and it is often computationally (and theoretically) simpler to design a sub-optimal one" [7]. Therefore, define γ_{min} such that

$$\gamma_{\min} = \min_K \left\|F_l(P,K)\right\|_\infty \tag{34}$$

such that *K* is a stabilizing controller. Then the H_∞ control problem becomes

$$\left\|F_l(P,K)\right\|_\infty < \gamma \tag{35}$$

where $\gamma > \gamma_{min}$. By reducing γ iteratively, an optimal solution can be approached.

4.3 Two Degrees-of-Freedom H_∞ Control Design

The design of H_∞ controllers consists of shaping the maximum singular value of certain transfer function matrices within a system over a frequency range. The choice of which transfer functions to shape is entirely left to the designer, with

choices ranging from minimizing control effort to minimizing disturbance effects within the system. The reason that two degrees-of-freedom H_∞ Control is chosen for this system is due to its ability to reject system disturbances, which is important in hydraulic control design. Also, the work of Bax [9] showed that this particular control architecture worked well when controlling a hydraulic valve assembly, encouraging the use of this control design in other hydraulic work.

The roots of two degrees-of-freedom H_∞ Control lie in the control designs of MacFarlane and Glover. Their MacFarlane-Glover H_∞ Loop-shaping design, while allowing only one degree of freedom, utilized a prefilter to meet steady-state tracking requirements. The work by Hoyle and Limebeer sought to redesign the MacFarlane-Glover H_∞ Loop-shaping into a true two degrees of freedom controller [7]. The architecture they chose allowed for the feedback portion of the controller to be designed to meet robust stability and disturbance rejection requirements except that only a pre-compensator weight is used. Schematics of the controlled system are shown in Figure 26 and Figure 27.

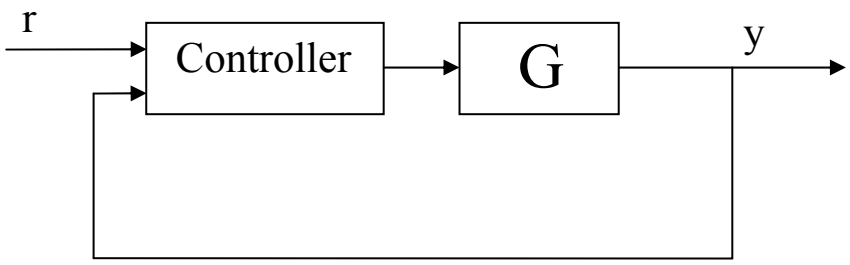

Figure 26. General two degrees-of-freedom control architecture

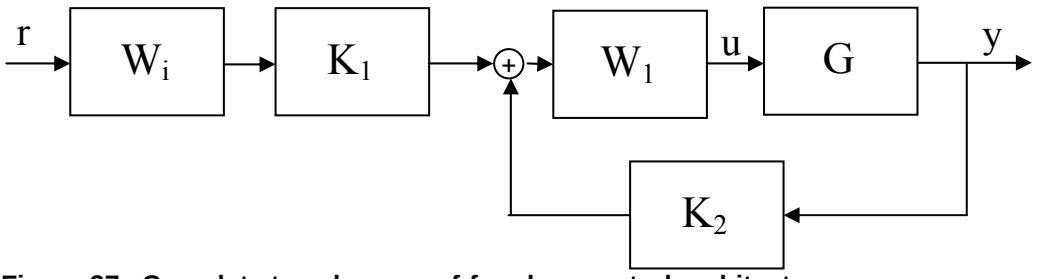

Figure 27. Complete two degrees-of-freedom control architecture

The design problem of this particular control scheme involves finding the stabilizing controller

$$K = \begin{bmatrix} K_1 & K_2 \end{bmatrix} \tag{36}$$

for the shaped plant

$$G_s = GW_1 \tag{37}$$

which minimizes the H_∞ norm of the transfer function between the input and output signals via the coprime factorization

$$G_s = M_s^{-1} N_s \tag{38}$$

To solve Eq. (38), the Matlab function *coprimeunc.m* [10] was utilized, available from Skogestad et al. [7]. The input to this function is the state-space representation of the shaped plant GW_1 and a relative tolerance term, typically set equal to 1.1. The output of the function is the state-space representation of the stabilizing controller, K.

The control signal applied to the shaped plant G_s is

$$u_s = \begin{bmatrix} K_1 & K_2 \end{bmatrix} \begin{bmatrix} \beta \\ y \end{bmatrix} \tag{39}$$

where β is the scaled reference, y is the measured output, and K_1 and K_2 are referred to as the prefilter and feedback controller, respectively. The task of the prefilter is to ensure that

$$\left\| (I - G_s K_2)^{-1} G_s K_1 - T_{ref} \right\|_\infty \le \gamma \rho^{-2} \tag{40}$$

where T_{ref} is the desired closed-loop transfer function and ρ is a scalar parameter used to place more or less emphasis on model matching at the expense of robustness. The reference model T_{ref} is used to incorporate time-domain specifications into the design process, such as a desired natural frequency of oscillation and damping ratio.

With the optimization routines nearly established, the generalized plant P must be defined. Assembly of the generalized plant can be performed from knowledge of the shaped plant and reference model, of the forms

$$G_s \overset{s}{=} \begin{bmatrix} A_s & B_s \\ C_s & D_s \end{bmatrix} \tag{41}$$

and

$$T_{ref} \overset{s}{=} \begin{bmatrix} A_r & B_r \\ C_r & D_r \end{bmatrix}. \tag{42}$$

The generalized plant is then

$$P = \begin{bmatrix} A_s & 0 & 0 & \left(B_s D_s^T + Z_s C_s^T\right) R_s^{-1/2} & B_s \\ 0 & A_r & B_r & 0 & 0 \\ 0 & 0 & 0 & 0 & I \\ C_s & 0 & 0 & R_s^{1/2} & D_s \\ \rho C_s & -\rho^2 C_r & -\rho^2 D_r & \rho R_s^{1/2} & \rho D_s \\ 0 & 0 & \rho I & 0 & 0 \\ C_s & 0 & 0 & R_s^{1/2} & D_s \end{bmatrix} \tag{43}$$

where Z_s is the unique positive definite solution to the generalized Riccati equation for the state-space representation G_s

$$(A - BS^{-1}D^T C)Z + Z(A - BS^{-1}D^T C)^T - ZC^T R^{-1} CZ + BS^{-1}B^T = 0 \tag{44}$$

and

$$R_s = I + D_s D_s^T . \tag{45}$$

To find a solution to this optimization, the Matlab routine *hinf2dof.m* [11] was used, which is available from Skogestand et al. [7].

The final portion of the controller is the prefilter gain W_i, used to ensure steady-state tracking. This gain is defined by

$$W_i \stackrel{\Delta}{=} \left[W_o \left(I - G_s(0) K_2(0) \right)^{-1} G_s(0) K_1(0) \right]^{-1} T_{ref}(0) , \tag{46}$$

where W_o is the output selection matrix, allowing the designer to choose between distinct system outputs to control. If no extra feedback measurements beyond those already controlled, exist, then $W_o=I$. The reason for this prefilter gain is that the previous optimization routine seeks only to minimize the ∞-norm of the error, not the actual error.

Chapter 5

PRESSURE CONTROL DESIGN

5.1 Performance Weighting

The objective of the study in this project and any control design study is to meet a set of performance requirements while maintaining stability. In this application, restrictions have been set in the time domain on allowable steady-state error and maximum overshoot. In the frequency domain, a restriction has been set on system bandwidth. These requirements are outlined in Table 3. Along with these requirements, it is necessary that the system does not oscillate when tracking a steady signal.

Table 3. Performance design objectives

Design Criteria	Design Objective
Bandwidth	2 Hz
Steady-State Error	5%
High Frequency Error	200%

The performance requirements outlined in Table 3 can be incorporated into a single transfer function requirement for use with the performance analysis in the frequency domain. These requirements are summarized in the performance weight,

$$w_P(s) = \frac{\frac{1}{M}s + \omega_B}{s + \omega_B A} \tag{47}$$

where M is the high frequency error in percent, A is the steady-state tracking error in percent, and ω_B is the bandwidth.

5.2 PID Controller Design and Implementation

To compare "modern" controllers to current techniques in hydraulic control, a controller representing classical control methods needs to be constructed. A PID controller representing a performance "baseline" can be quickly formulated using classical design methods.

The input to a PID controlled plant is calculated as

$$u = k_P e + k_I \int e\,dt + k_D \frac{de}{dt} \tag{48}$$

where k_P is the proportional control term, k_I is the integral control term, and k_D is the derivative control term. The algorithm for designing a PID controller consists of choosing each of these three parameters individually.

The first step of control design is the analysis of the plant that is to be controlled. The linear plant analyzed in Section 2.3 is stable, making the design task simpler. Even if the plant were unstable, control design would still be possible. Recall that the input to the model is the current input to the control valve and the output of the system is the pump discharge pressure.

To analyze the controllability of the linear model, a Bode diagram of the open-loop model is constructed, shown in Figure 28. Note that while the gain margin of the plant is infinite, the phase margin is roughly 135º. This is encouraging, as a phase margin greater than zero generally translates to a controllable system. Another important piece of information learned from Figure 28 is that the plant is closed-loop

stable. What this means is that a control gain of K=1 would yield a stable system, although with poor performance characteristics.

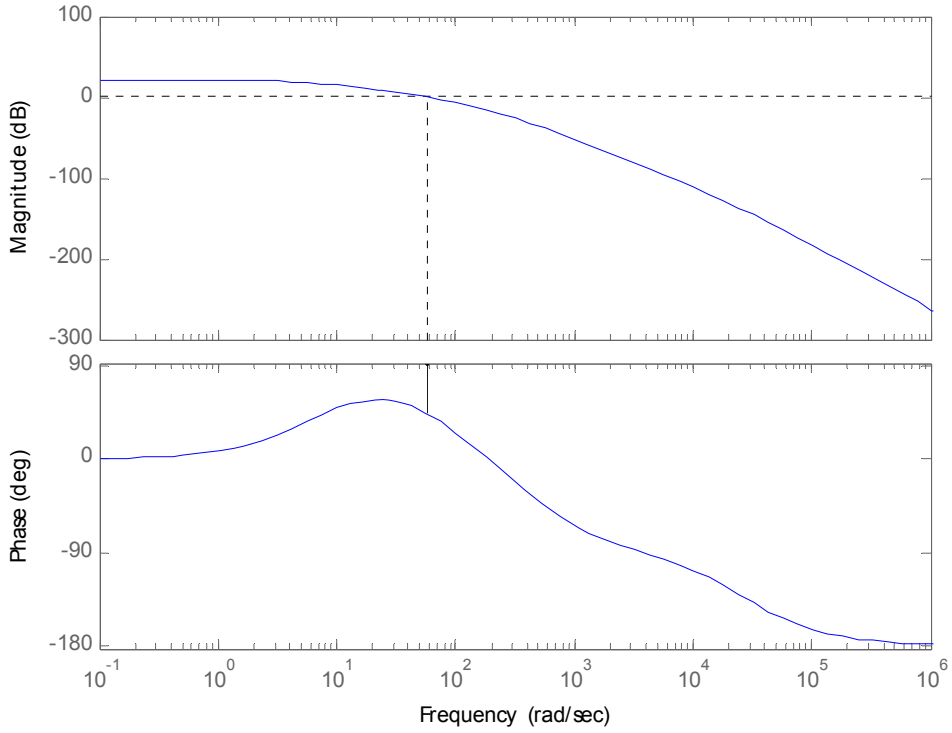

Figure 28. Bode diagram of the open-loop plant

The addition of a controller gain should improve the performance characteristics of the system even further. To design a PID controller, a proportional gain alone is first selected to control the system. The reason for this is that a proportional controller is relatively simple, and if it alone has the ability to control a system to meet its design goals, it should be used. However, the disadvantages of using a proportional controller to manage a hydraulic pump will be shown.

The proportional gain was chosen as k_P=0.05 simply as a starting point. The reason for this choice is that the current input to the control valve is on the order of 1

Amp, while the pump pressure is on the order of 10's of MPa. A quick calculation yields an approximate control resolution on the order of 0.5 Amps, which is within the sensitivity range of the system. The time domain response of the pump pressure with proportional control is shown in Figure 29. The reference input is a step function. For $0 < t < 1$s, the reference input is equal to 5.0 MPa. For $t > 1$s, the reference input is equal to 5.2 MPa.

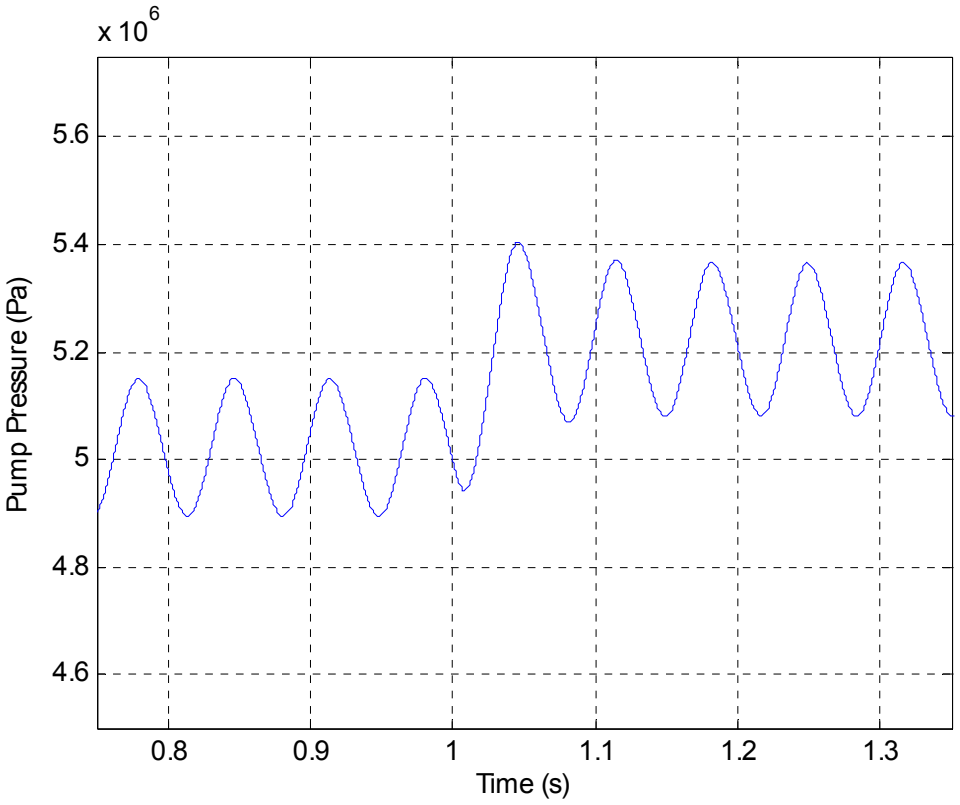

Figure 29. Proportionally controlled system response to a step input

Upon studying Figure 29, several conclusions can be made about the proportional control system. First, the system oscillates as it tracks the reference signal, a condition clearly outlined as unacceptable in Section 3.1. Secondly, the

system appears to oscillate about the reference signal, meaning that the system could possess desirable tracking properties if the output oscillation could be removed.

Generally, to remove oscillation from a controlled system, the derivative term k_D is added to the PID controller. The reason for this is that derivative control works to drive the derivative of the error signal to zero. If the derivative of the error is equal to zero, then the error does not change as a function of time, removing oscillatory behavior from the system.

As a general rule, the derivative control term in a PID controller is initialized as one tenth of the proportional control. While this value is merely a starting point in control design, there is a valid reason for this scale. The addition of derivative control tends to de-stabilize a controlled system, due to the fact that the derivative control portion of the PID controller only responds to the derivative of the error in the system, not to the actual error. This property can sometimes cause the derivative controller to resist the efforts of the proportional controller in the system, impairing system performance.

The derivative control term k_D was chosen to be 0.005. The response of the system with proportional and derivative (PD) control is shown in Figure 30. With the oscillatory behavior removed, the system can be more readily studied.

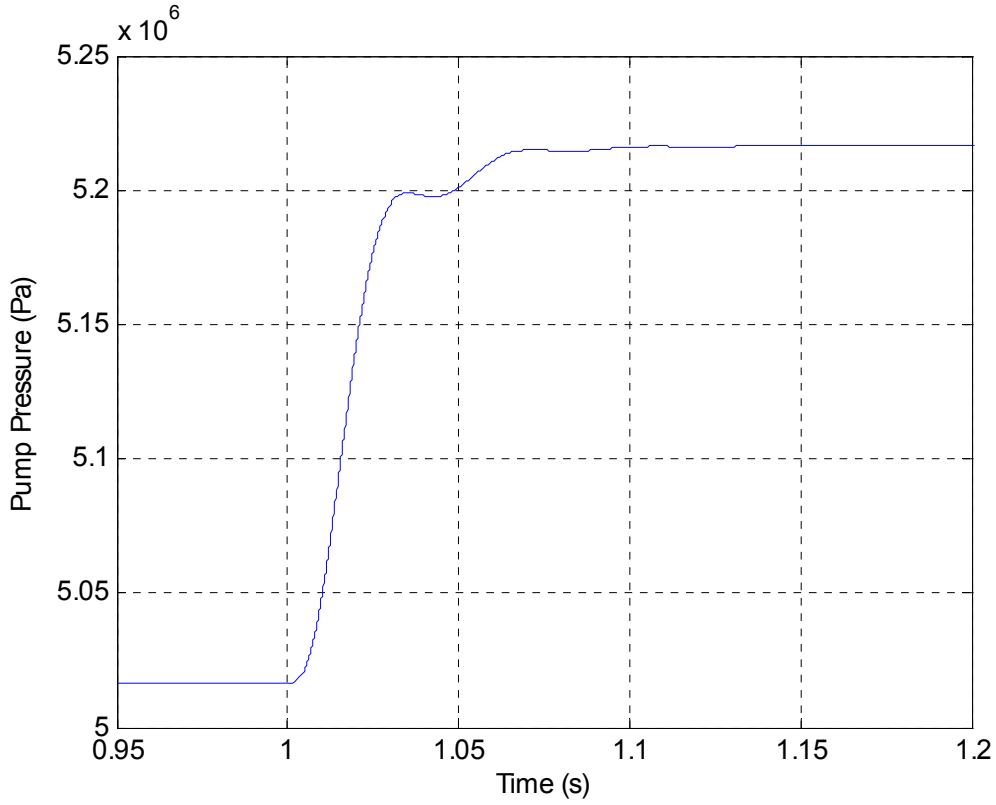

Figure 30. PD controlled system response to a step input.

From observing Figure 30, several conclusions can be made. First, the steady-state error requirement from Section 3.1 has been satisfied. Satisfaction of this requirement may seem surprising without the inclusion of integral control. However, the work of Manring [6] supports this conclusion, as he states that a variable displacement hydraulic pump possesses integral-like behavior, allowing a pump control design to require at most a PD control scheme.

The second conclusion that can be made is that the performance output response has no overshoot. This overdamped response is a very important quality of successful pump controllers, as overshoot is proportional to the change in pump

pressure. For large and sudden changes in commanded pump pressure, large amounts of overshoot can be dangerous to both system components and operators.

Upon completion of the time domain analysis of the PD controlled system, frequency domain analysis can begin. The Bode diagram of the open-loop controlled system is shown in Figure 31. Notice that the phase margin of the system has been improved from 135º to nearly 180º. This increase translates to better performance characteristics and greater robustness to variation. Also, notice that the phase margin is near its maximum possible value under the current control scheme. When the phase margin of a controlled system has been maximized, the controller has been optimized for performance. Therefore, no additional controller tuning is necessary.

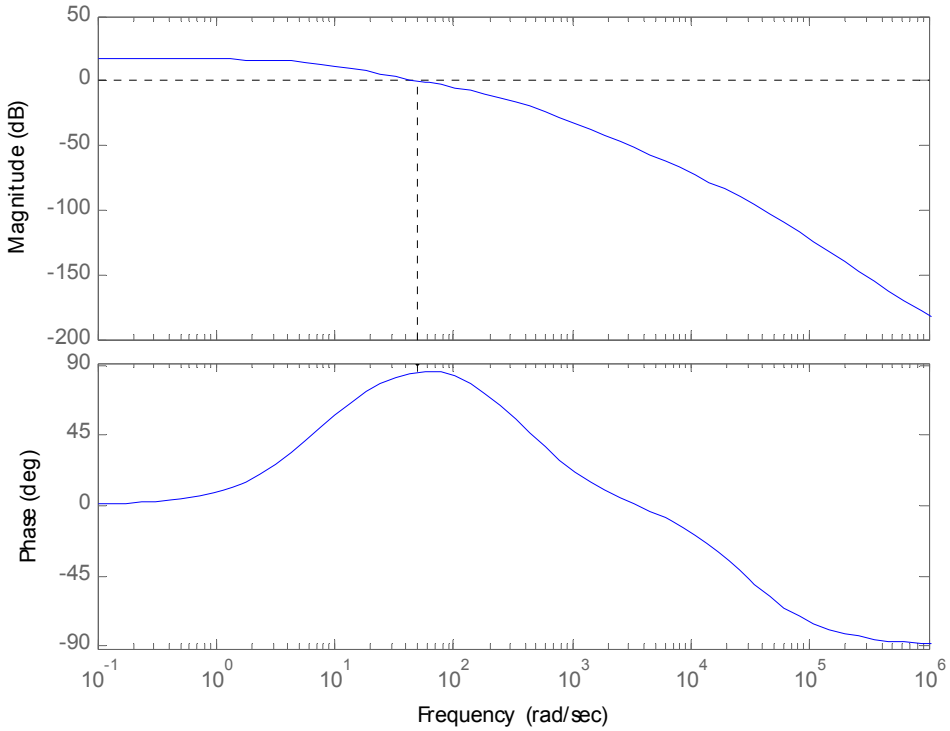

Figure 31. Bode diagram of the open-loop PD controlled system

5.3 Two Degrees-of-Freedom H_∞ Controller Implementation

In essence, many controllers possess two degrees of freedom in their design. Measured signals provide one degree while the reference signal provides the other. Often, one of these degrees of freedom is lost by driving the controller with the system error (the difference between the measured output and the reference input). However, reclaiming this degree of freedom by conditioning the reference input can enable the system to achieve better performance and increased robustness properties. The schematic of the two degrees-of-freedom control system is shown in Figure 26. By conditioning the reference input, the designer may set performance characteristics for the controlled system response. The conditioning transfer function in the system uses an existing PID controller for the plant, designed purely for performance and not robustness, to define the desired closed-loop response of the controlled plant.

The reference model, possessing the desired closed-loop response characteristics, is defined by

$$T_{ref}(s) = \frac{\omega_n^2}{s^2 + 2\zeta\omega_n s + \omega_n^2}. \tag{49}$$

By defining the reference model in this fashion, the damping ratio and natural frequency of the desired system can be clearly defined. The desired natural frequency of the pump pressure response is 2 Hz, and the desired damping ratio is 0.707. A unit-step response of the reference model is shown in Figure 32. The model matching factor ρ from Eq. (40) is set to 1.1 for the duration of the control design process.

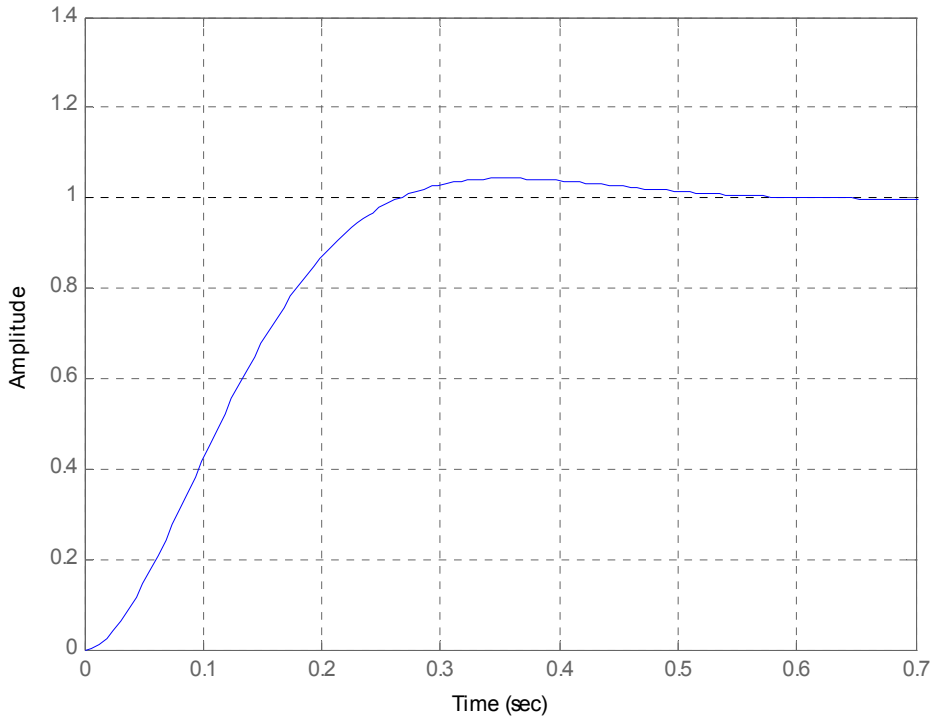

Figure 32. Step response of the reference model, T_{ref}

The dynamic characteristics defined by the reference model appear to be present in Figure 32. The percent overshoot of the response is 5% with no steady-state error. The controlled response of the linear model using the two degrees-of-freedom controller is shown in Figure 33.

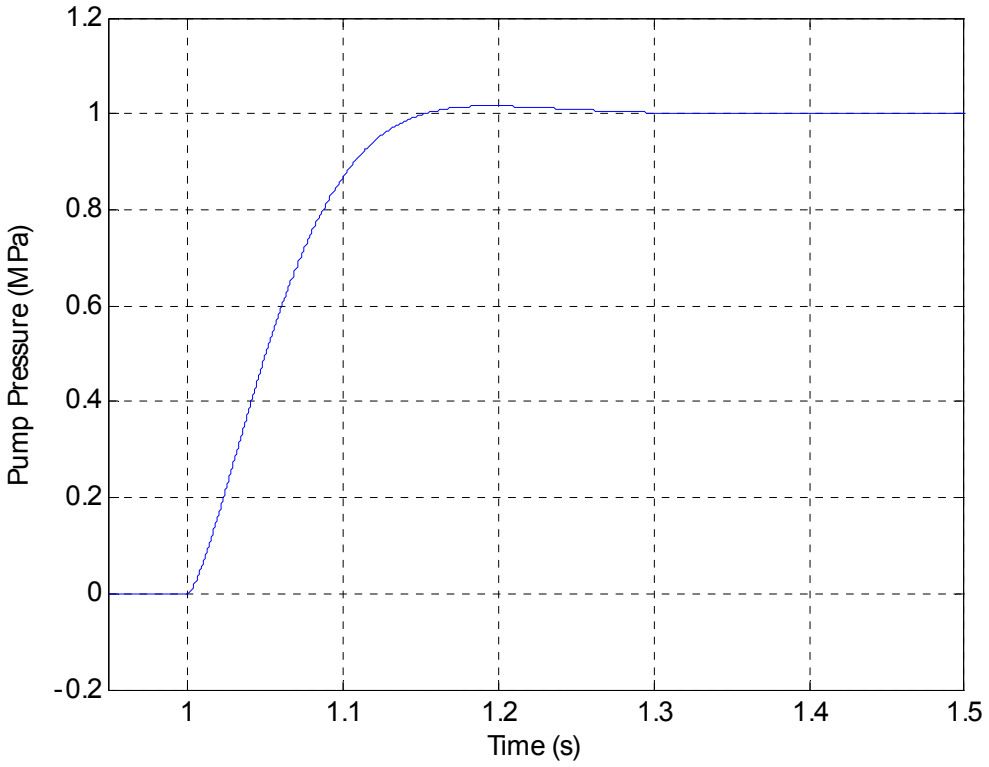

Figure 33. Linear response of the two degrees-of-freedom controlled model

Again, the percent overshoot of the system is roughly 5% with no steady-state error, matching the reference model well. The controlled response of the nonlinear system is shown in Figure 34.

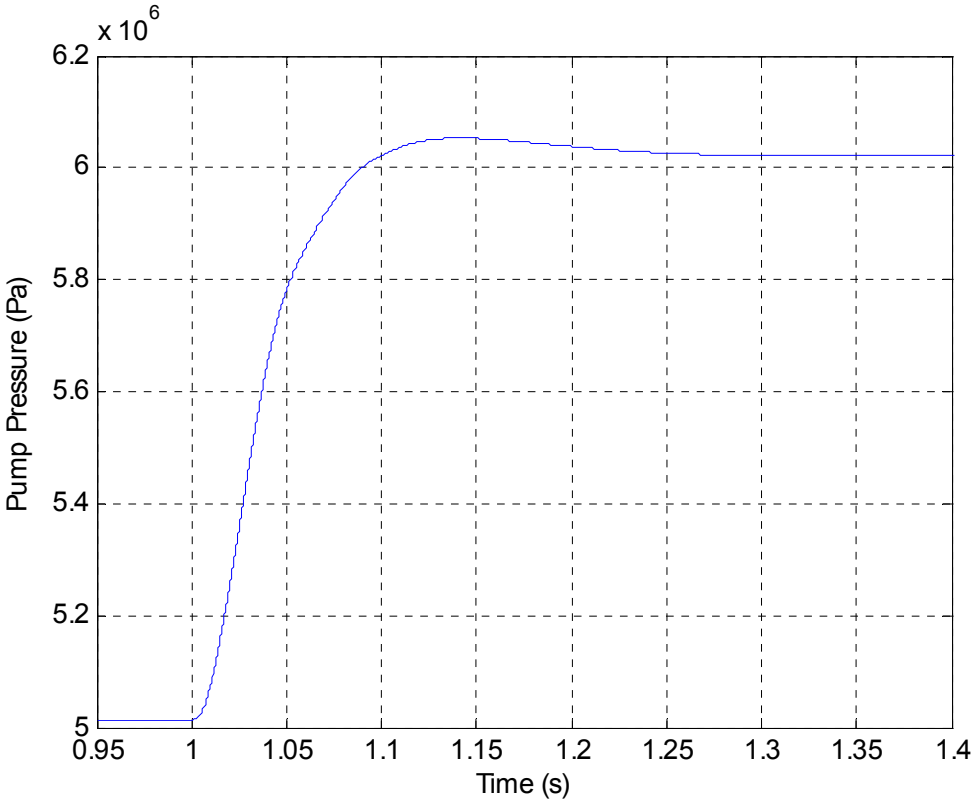

Figure 34. Nonlinear response of the two degrees-of-freedom controlled system

Once again, the overshoot of the nonlinear system is roughly 5%, with slight steady-state error. This error is within the acceptable bound for this control study.

The disadvantage of using modern controller techniques, often, is that the controllers produced are of high order. The pole-zero map of the 14th-order two degrees-of-freedom controller is shown in Figure 35.

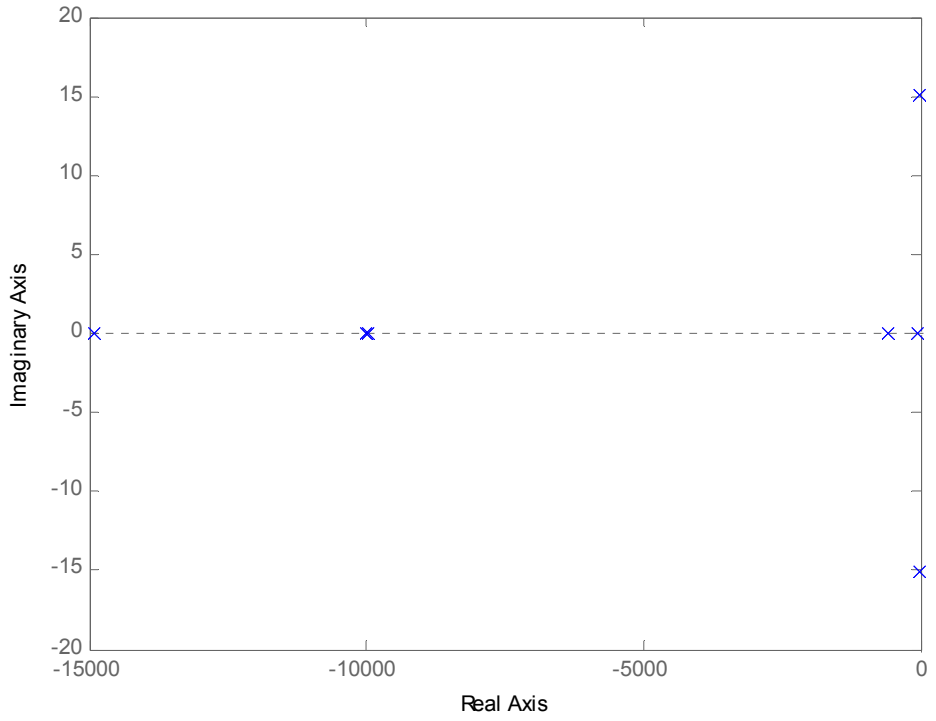

Figure 35. Pole-zero map of the original two degrees-of-freedom controller

Based on Njabeleke's work [1], showing that higher-order modern controllers can be reduced in order with little loss of precision, model order reduction was employed on the high-state controller using the Matlab utility *minreal.m*. The pole-zero map of the 6^{th} order revised two degrees-of-freedom controller is shown in Figure 36.

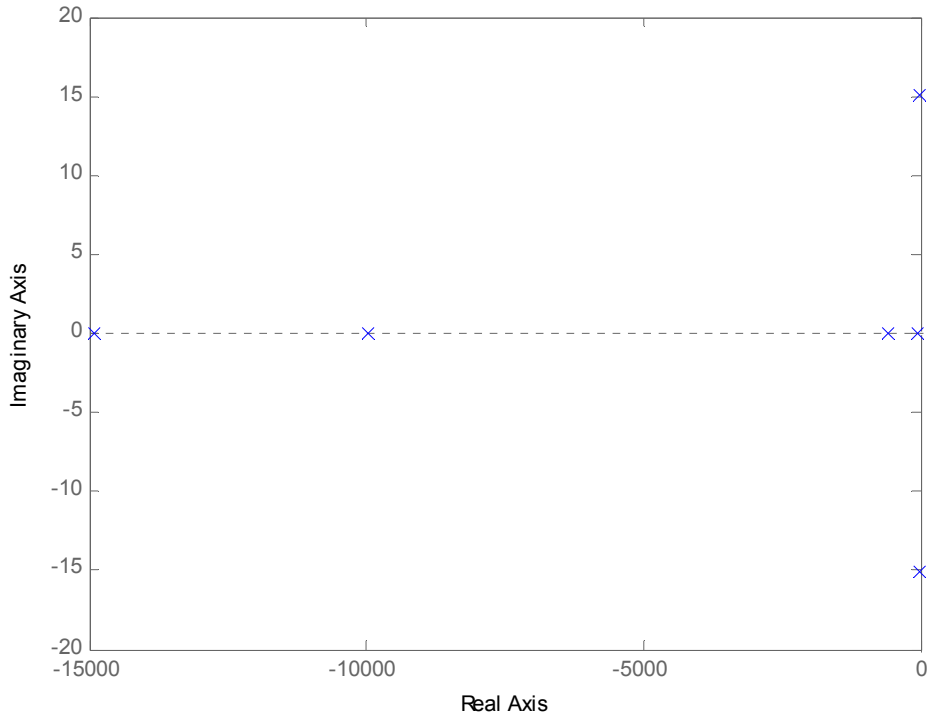

Figure 36. Pole-zero map of the order-reduced controller

While no exceptionally fast poles were removed from the system, the reduction of the order of the controller will help reduce computational requirements. Additional order reduction can be achieved using a second *Matlab* utility, *sresid.m*, available from [7]. This routine allows the designer to choose the number of system poles (and therefore states) to remove from the system, beginning with the fastest pole. This routine was used to first reduce the high order controller gain K_2, from Eq. (39), with little loss of accuracy. However, use of routines such as *sresid.m* can lead to a loss of precision between order reductions. If the reduction is too severe, the resulting system may possess unwanted controller dynamics. When further order reduction was attempted on the controller shown in Figure 36, this loss of precision was observed, and thus

this sixth-order controller was used for the duration of the modern controller analysis in this study. The design of the two degrees-of-freedom controller is shown in its entirety in Appendix A.

Chapter 6

FREQUENCY DOMAIN ANALYSIS OF ROBUSTNESS

6.1 Robustness Definitions in the Frequency Domain

While the idea of robustness might at first seem abstract, there are mathematical techniques for quantifying the robustness of a system using the frequency response of the system. Certain robustness characteristics can be defined and analyzed to compare different control schemes. These robustness characteristics are summed up in four categories: nominal stability, nominal performance, robust stability and robust performance. While nominal stability (NS) might not be defined as a measure of robustness, it is generally thought of as the starting point in all control research. Nominal performance (NP), then, verifies whether or not the nominal controlled system meets the desired performance requirements. Robust stability (RS) determines whether or not the control system is stable for all perturbations of the model. Robust performance (RP) verifies whether or not the performance and stability criteria are met for all perturbations of the model. These characteristics are then evaluated in the frequency domain. The magnitude of each of these requirements is examined to determine if the system satisfies the requirement.

To begin analyzing robustness, several notations must first be explained. First, the system matrix N is created using a block diagram manipulation of the generalized plant model P and the controller K. This arrangement can be seen schematically in Figure 37. Mathematically, P and K are joined using a lower linear fractional transformation.

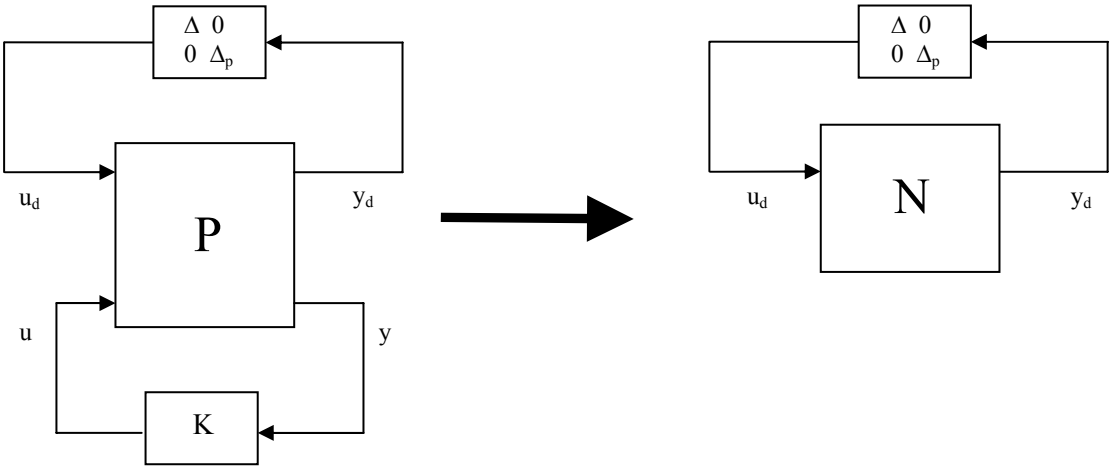

Figure 37. Lower linear transformation schematic

The system matrix N is then defined as

$$N = F_l(P,K) \equiv P_{11} + P_{12}K(I - P_{22}K)^{-1}P_{21} \tag{50}$$

It should be noted that both the first input and first output of the system matrix N are vector signals, due to the structured uncertainty model. For a lumped uncertainty model, these signals are scalars. The final notation necessary is that of the structured singular value μ. The structured singular value is used in place of the singular value σ in an attempt to take advantage of the diagonal structure of the uncertainty description, versus an unstructured uncertainty description [7]. The structured singular value of a plant G is then defined as

$$\mu_\Delta(G) = \left(\min\left\{k_m \middle| \det(I - k_m G\Delta) = 0 \text{ for structured } \Delta, \bar{\sigma}(\Delta) \le 1\right\}\right)^{-1} \tag{51}$$

where k_m is the scaling factor that allows

$$\det(I - k_m G\Delta) = 0\,. \tag{52}$$

With these definitions in place, the robustness properties of a controlled system can be outlined. The derivations for each of these properties can be found in [7]. The robustness properties are defined as:

$$NS \leftrightarrow N \text{ is stable} \tag{53}$$

$$NP \leftrightarrow \bar{\sigma}(N_{22}) = \mu_{\Delta p} < 1 \quad \forall \omega \tag{54}$$

$$RS \leftrightarrow \mu_{\Delta}(N_{11}) < 1 \quad \forall \omega \tag{55}$$

$$RP \leftrightarrow \mu_{\hat{\Delta}}(N(j\omega)) < 1 \quad \forall \omega, \tag{56}$$

where

$$\hat{\Delta} \equiv \begin{bmatrix} \Delta & 0 \\ 0 & \Delta_p \end{bmatrix}. \tag{57}$$

The determination of nominal stability (NS) was made by analyzing the pole-zero map of each controlled system and observing pole location. Nominal stability of each controlled system will not be discussed further.

6.2 Robust Analysis of PID Controlled System

To be able to analyze the robustness characteristics of the PID controller in the frequency domain, the structured uncertainty model must be added to the generalized plant *P*. Figure 38 shows the block diagram structure of the generalized plant with structured uncertainty.

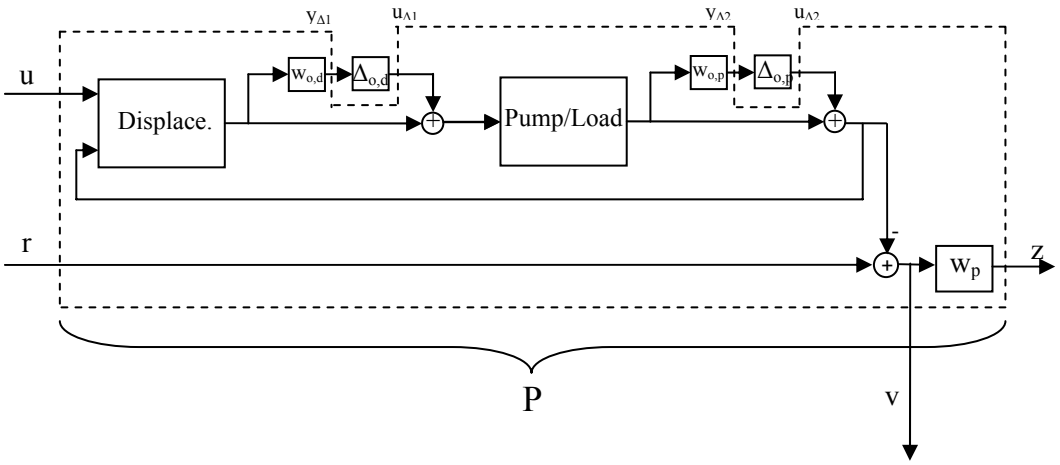

Figure 38. Generalized plant model with uncertainty

It is important to note at this point the structural difference between the lumped uncertainty description and the structured uncertainty description, in terms of robustness analysis. In Eq. (57), the Δ-block structure for the structured uncertainty model is written as

$$\hat{\Delta} = \begin{bmatrix} \Delta_{o,d} & 0 & 0 \\ 0 & \Delta_{o,p} & 0 \\ 0 & 0 & \Delta_p \end{bmatrix}, \tag{58}$$

while the corresponding Δ-block structure for the lumped uncertainty case would be expressed as

$$\hat{\Delta} = \begin{bmatrix} \Delta & \Delta & 0 \\ \Delta & \Delta & 0 \\ 0 & 0 & \Delta_p \end{bmatrix}. \tag{59}$$

The fact that all off-diagonal elements of the structured Δ-block are zero ensures that the uncertainty of a system component affects only that component. In the case of lumped uncertainty, the non-zero off-diagonal terms allow the uncertainty of separate system components to affect each other.

The generalized plant then consists of a set of dynamic equations, each represented by transfer functions. The system equations are

$$u_{\Delta 1} = \left(\frac{V w_{o,d} D_2}{1 - D_2 V}\right) y_{\Delta 1} + \left(\frac{w_{o,d} D_2}{1 - D_2 V}\right) y_{\Delta 2} + (0) r + \left(\frac{w_{o,d} D_1}{1 - D_2 V}\right) u \tag{60}$$

$$u_{\Delta 2} = \left(\frac{w_{o,v} V}{1 - D_2 V}\right) y_{\Delta 1} + \left(\frac{w_{o,v} V D_2}{1 - D_2 V}\right) y_{\Delta 2} + (0) r + \left(\frac{w_{o,v} V D_1}{1 - D_2 V}\right) u \tag{61}$$

$$z = \left(\frac{-V w_p}{1 - D_2 V}\right) y_{\Delta 1} + \left(\frac{-w_p}{1 - D_2 V}\right) y_{\Delta 2} + (w_p) r + \left(\frac{-D_1 V w_p}{1 - D_2 V}\right) u \tag{62}$$

$$v = \left(\frac{-V}{1 - D_2 V}\right) y_{\Delta 1} + \left(\frac{-1}{1 - D_2 V}\right) y_{\Delta 2} + (I) r + \left(\frac{-D_1 V}{1 - D_2 V}\right) u \tag{63}$$

where D is the linearized displacement model and V is the linear model of the pump/load valve assembly. The specifications D_1 and D_2 represent subcomponents of the displacement model in which either the first or second input, respectively, is considered alone. Therefore, the model D_1 is the linearized displacement model considering only the current input and D_2 is the linearized displacement model considering only the pump pressure input, such that

$$D = \begin{bmatrix} D_1 & D_2 \end{bmatrix}. \tag{64}$$

The resulting generalized plant P_{PID} is defined by

$$P_{PID} = \begin{bmatrix} \frac{Vw_{o,d}D_2}{1-D_2V} & \frac{w_{o,d}D_2}{1-D_2V} & 0 & \frac{w_{o,d}D_1}{1-D_2V} \\ \frac{w_{o,v}V}{1-D_2V} & \frac{w_{o,v}VD_2}{1-D_2V} & 0 & \frac{w_{o,v}VD_1}{1-D_2V} \\ \frac{-Vw_p}{1-D_2V} & \frac{-VD_2w_p}{1-D_2V} & w_p & \frac{-D_1Vw_p}{1-D_2V} \\ \frac{-V}{1-D_2V} & \frac{-1}{1-D_2V} & 1 & \frac{-D_1V}{1-D_2V} \end{bmatrix}. \quad (65)$$

After employing the lower linear fractional transformation with the PID controller shown in Figure 37, the system matrix *N* was calculated. By using the robustness tests shown in Eqs. (54 – 56), the robustness characteristics of the PID controlled model are shown in Figure 39.

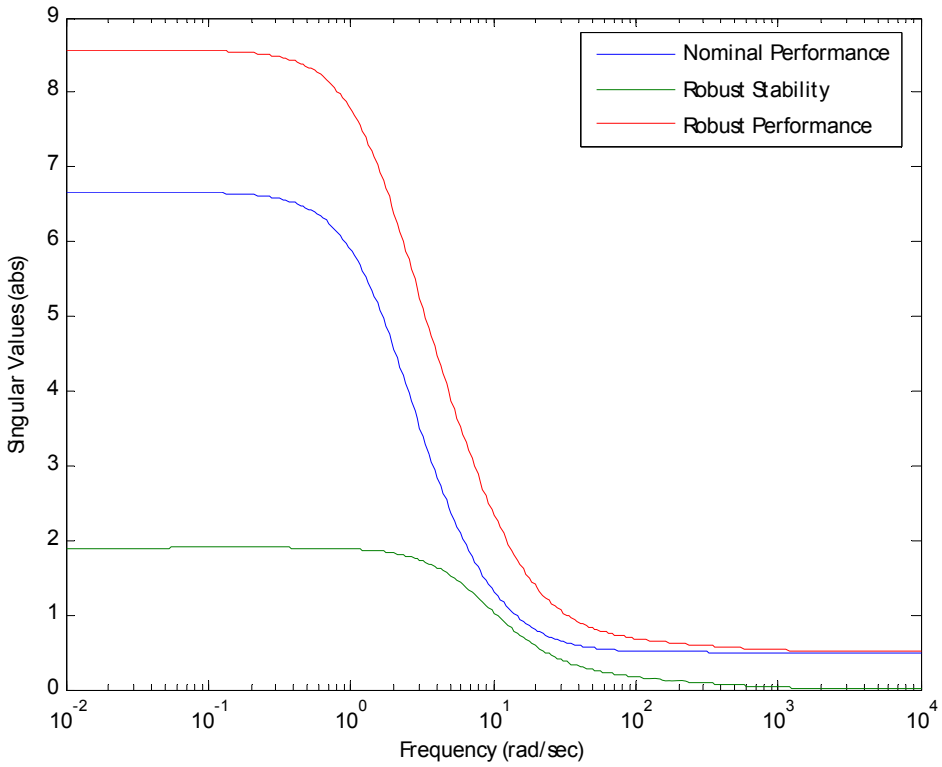

Figure 39. Robustness characteristics of the PID controlled plant

The robustness characteristics shown in Figure 39 tell a great deal about the PID controlled system. The nominal performance criteria does not pass the test outlined in Eq. (54), with a low frequency maximum near 7. This means that the system is not expected to satisfy the performance constraints laid out in Section 5.1 under nominal operating conditions. The robust stability shown also does not satisfy the criteria from Eq. (55), meaning that the model is not expected to maintain stability under all system variations. Finally, the robust performance criterion shown does not meet the qualifications of Eq. (56), meaning that the system is not expected to meet the performance requirements under all system variations. However, these three

characteristics can be used as metrics to judge the stability or performance of a control system when compared with another control system.

6.3 Comparing Robustness between Lumped and Structured Uncertainty Models

At this point it is interesting to analyze the effects of the structured uncertainty model, derived in Chapter 3. In that chapter, the decision was made to pursue a structured uncertainty model to ensure a certain level of accuracy in robustness analysis. The lumped uncertainty model shown in Figure 20 was determined to be too conservative, and the structured uncertainty model shown in Figure 23 and Figure 24 was chosen for eventual robustness analysis.

While the robustness characteristics of the PID controlled system employing structured uncertainty were outlined in the previous section, this same analysis can be quickly applied to the model assuming that a lumped uncertainty model is used. The generalized plant P of the system with lumped uncertainty is

$$P = \begin{bmatrix} 0 & 0 & w_o G \\ w_p & -w_p & -w_p G \\ 1 & -1 & -G \end{bmatrix}, \tag{66}$$

as derived from the block diagram structure shown in Figure 40. The resulting robustness analysis is shown in Figure 41.

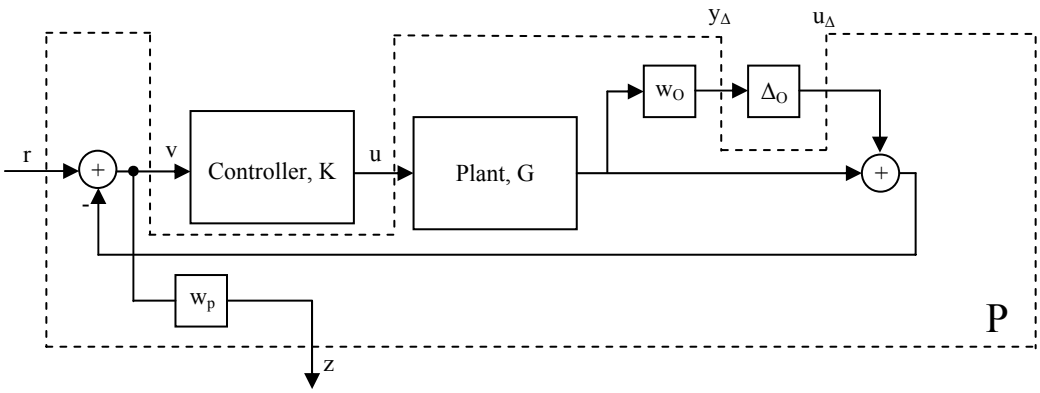

Figure 40. Generalized plant structure with lumped uncertainty model

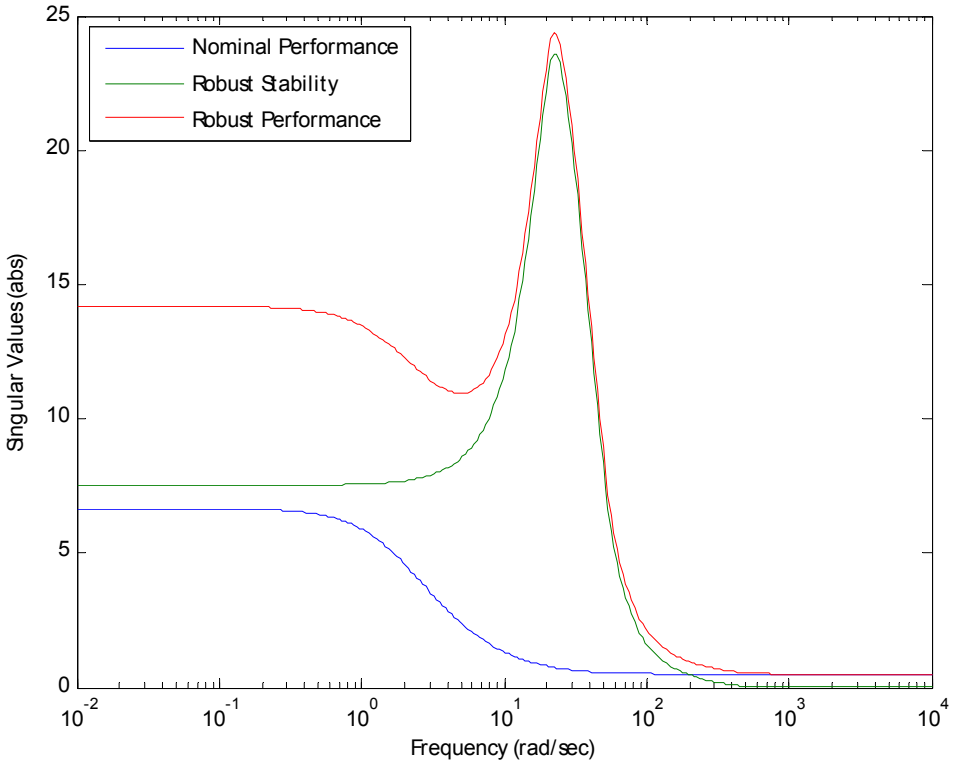

Figure 41. Robustness analysis of PID controlled system with lumped uncertainty model

The nominal performance test result shown in Figure 41 is consistent with the findings from the structured uncertainty trial of the previous section. This makes sense, since the uncertainty of a system is unrelated to the nominal performance

properties of the system. The robust stability displayed, however, differs greatly from the results of the structured uncertainty case. The overly conservative lumped uncertainty model results in a robust stability measure of 8.00, more than four times less favorable than the structured uncertainty model. Because the structured uncertainty model is more accurate than the lumped uncertainty model, the robust stability measure using structured uncertainty is more accurate than its lumped uncertainty counterpart. What this means to the designer is that the controller in question is more robust than the lumped uncertainty model can relate, allowing for greater design freedom when using the structured uncertainty model.

6.4 Robust Analysis of Two Degrees-of-Freedom H_∞ Controlled System

To analyze the two degrees-of-freedom control system, only the structured uncertainty case was analyzed. The generalized plant *P* for the two degrees-of-freedom H_∞ controller is calculated from the controller architecture shown in Figure 42.

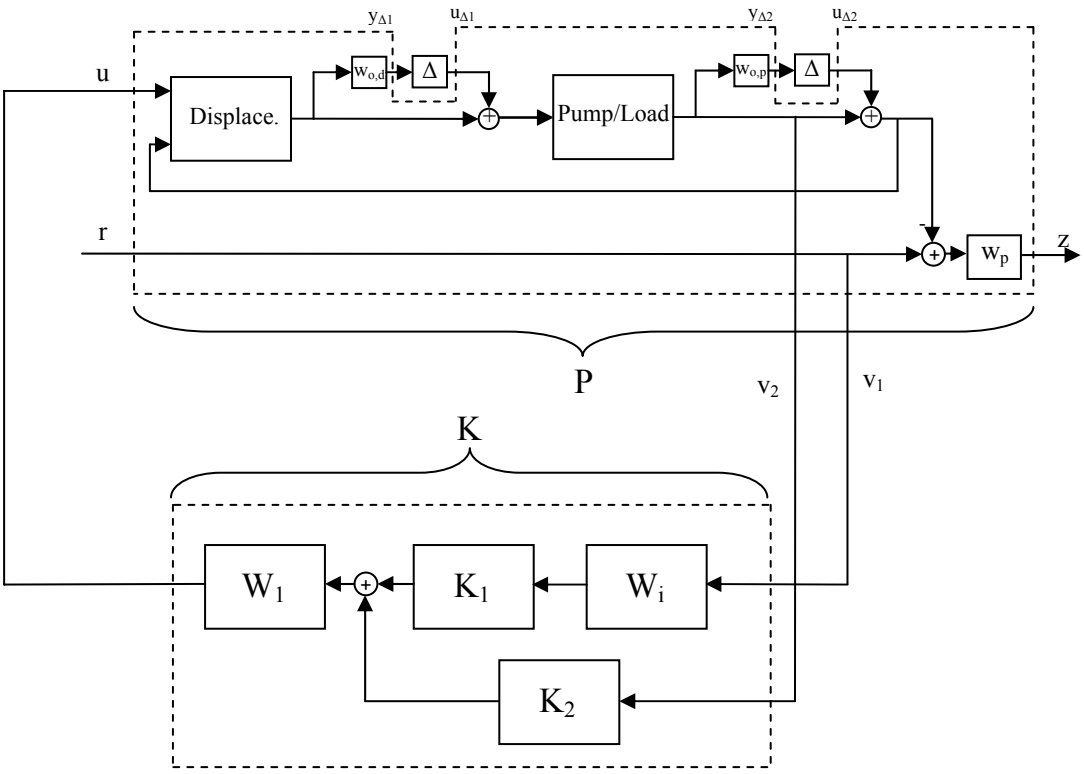

Figure 42. Block structure of two degrees-of-freedom controlled system

Using this structure, the generalized plant is defined by

$$P_{2DOF} = \begin{bmatrix} \frac{Vw_{o,d}D_2}{1-D_2V} & \frac{w_{o,d}D_2}{1-D_2V} & 0 & \frac{w_{o,d}D_1}{1-D_2V} \\ \frac{w_{o,v}V}{1-D_2V} & \frac{w_{o,v}VD_2}{1-D_2V} & 0 & \frac{w_{o,v}VD_1}{1-D_2V} \\ \frac{-Vw_p}{1-D_2V} & \frac{-VD_2w_p}{1-D_2V} & w_p & \frac{-D_1Vw_p}{1-D_2V} \\ 0 & 0 & 1 & 0 \\ \frac{-V}{1-D_2V} & \frac{-I}{1-D_2V} & 1 & \frac{-D_1V}{1-D_2V} \end{bmatrix} \quad (67)$$

The lower linear fractional transformation for this system is calculated in the same fashion as that for the PID controlled system of the previous section, with the exception that the reference input of the system acts as a second input to the controller *K*. The robustness characteristics of this system are analyzed in the same manner as in the PID controlled system. The graphical representation of the two degrees-of-freedom robustness characteristics is shown in Figure 43.

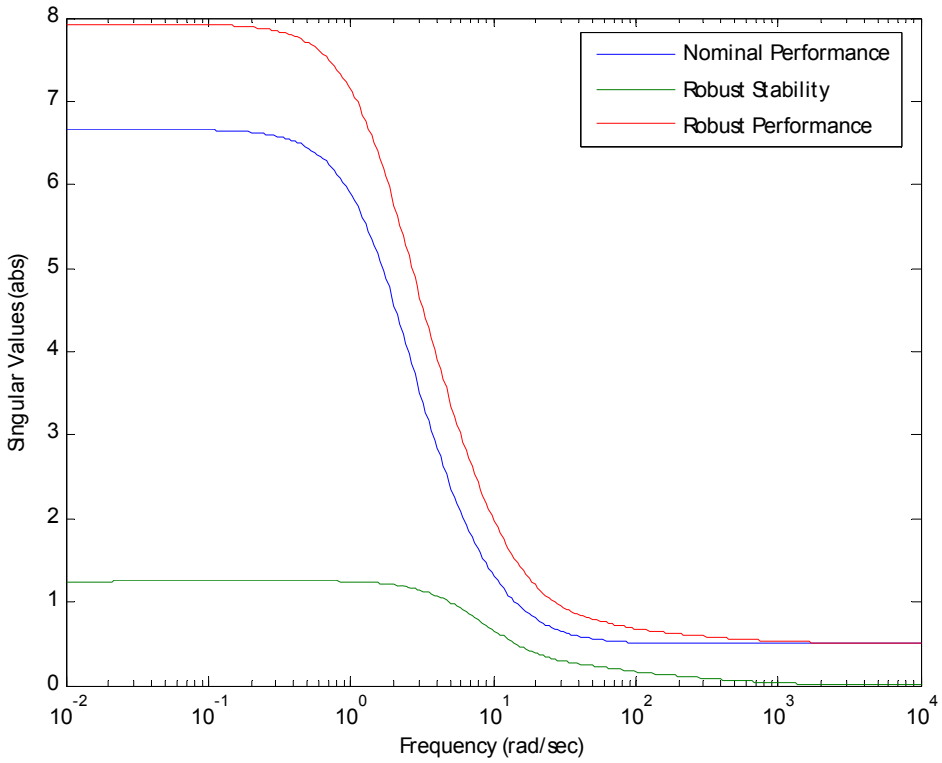

Figure 43. Robustness characteristics of the two degrees-of-freedom controlled system

Analysis of Figure 43 reveals several characteristics of the modern controlled system. Like the classically controlled system, the modern controlled system does not pass any of the three robustness tests. However, improvements over the PID controlled system have been made in the two metrics Robust Stability and Robust Performance.

6.5 Frequency Analysis Conclusions

Table 4 summarizes the results of the frequency domain tests on both control systems.

Table 4. Summary of frequency analysis robustness characteristics

Control Design	Robustness Test, Maximum Result (abs.)		
	Nominal Performance	**Robust Stability**	**Robust Performance**
PID Control	6.70	1.90	8.60
Two Degrees-of-Freedom Control	6.70	1.25	7.95

The information contained in Table 4 shows that the modern control scheme, while it does not pass any of the three robustness tests, does improve upon the PID controller in terms of robustness. The modern controlled system does not, however, improve over the PID controlled system in terms of Nominal Performance. This is expected, as the two degrees-of-freedom controller was built around the same PID controller designed in Section 5.2. This classical controller was designed with an emphasis on performance, not robustness. Therefore, only improvements on its design could be made in the area of robustness. In the time domain, this robustness increase translates to a more predictable system response in the face of variation. Time domain simulations of these controllers are presented in Chapter 7.

Chapter 7

TIME DOMAIN ANALYSIS OF ROBUSTNESS

7.1 Altered Models

To be able to analyze the uncertainty of a system in the time domain, varying models must be created. These models simulate the effects of parameter variation and disturbances in the hydraulic system. The parameters mentioned in the uncertainty analysis in Chapter 3 are the most logical candidates for variance, and will be explored here.

The most relevant issue to investigate in the field of hydraulics is the effect of a disturbance to the system. The uncertainty model included two parameters which could experience a perturbation. The fluid bulk modulus can be affected by many different system characteristics, some suddenly. The load valve area can also experience sudden changes as a consequence of hydraulic implement movement. Another source of variation that could affect time responses is the control valve within the pump. It has been shown in Chapter 3 that variations within this piece of equipment can cause the system to vary, even more than parameter variations.

Two time domain robustness tests were administered. First, a model variation test was run to study the responses of the controlled systems to different system models. These trials allowed parameters such as the fluid bulk modulus and the load valve area to vary between trials.

The second robustness test studied the effects of instantaneous changes in the load valve area. After the system was allowed to reach steady-state (i.e. a constant

discharge pressure), the load valve was perturbed from an opening of 3.5 cm^2 (70% open) to 5.0 cm^2 (100% open) and then to an opening of 2.0 cm^2 (40% open). This effect was simulated instantaneously, allowing for robustness analysis to be performed under ideal circumstances. The fluid bulk modulus was not perturbed in this fashion. This is because the system is operating at steady-state, at which point the pressure rise rate equations (Eq. (2)) are equal to zero. The fluid bulk modulus has an impact on the system only through these pressure equations, meaning that the impact of the fluid bulk modulus can only be observed during the transient response.

The results of these two robustness tests are analyzed differently from one another. The results of the model variation tests are compared for the specific controlled system involved, meaning that the robustness of the system is represented by how similarly the controlled system reacts under differing operating conditions. This can be thought of as a test of individual robustness. The parametric fluctuation test, however, can be analyzed most easily by comparing the reactions of the separately controlled systems with one another. If one system reacts more favorably than another (i.e. parameter fluctuation has less effect on the output), then that system is said to have greater robustness relative to the other, less favorable, control system.

7.2 Time Domain Responses

The time domain responses of the two controlled systems for a varying bulk modulus are shown first. In Figure 44 and Figure 45, the fluid bulk modulus was varied as noted, while the systems attempt to track a discharge pressure of 5 MPa from $0 < t < 1$ second, and a discharge pressure of 5.2 MPa for $t > 1$ second. Figure

44 concerns the PID controlled system, while Figure 45 concerns the two degrees-of-freedom controlled system.

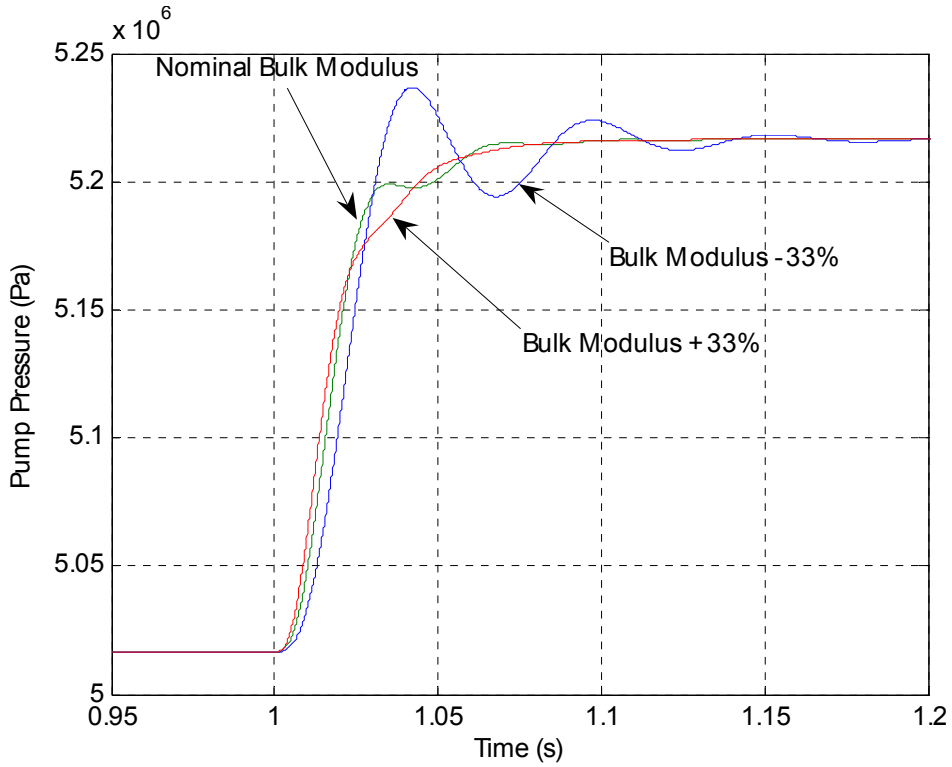

Figure 44. Variation of the PID controlled system for changing bulk modulus

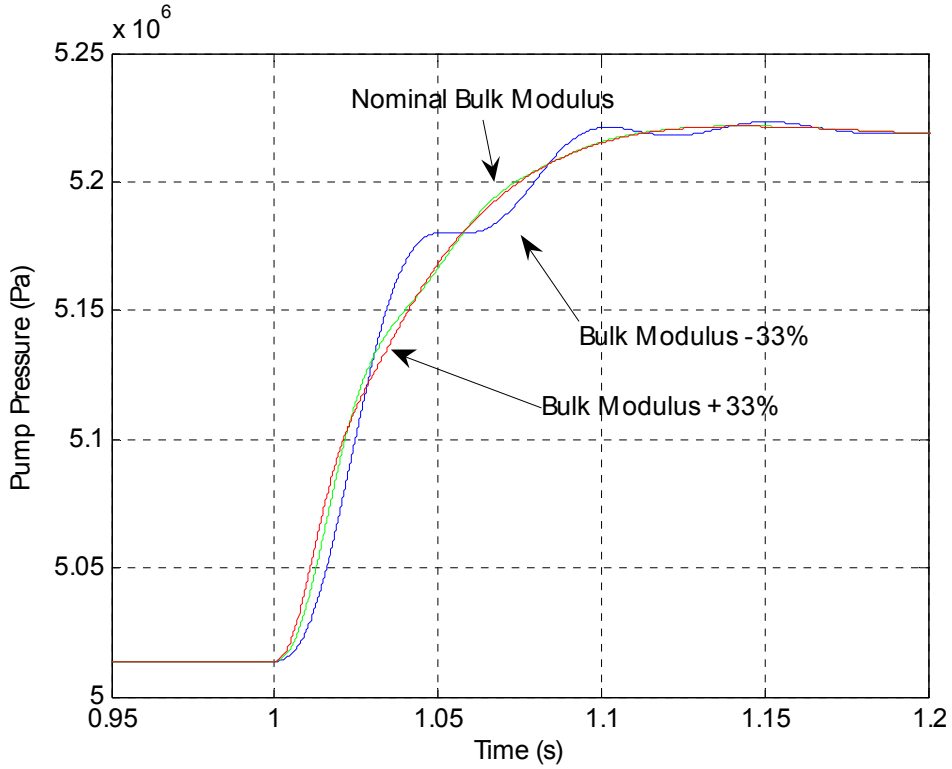

Figure 45. Variation of the Two DOF controlled system for changing bulk modulus

Upon comparing Figure 44 and Figure 45, it can be concluded that the PID controlled system response varies more than the modern controlled system as the bulk modulus changes between trials. While the average rise time of the PID controlled system is faster (0.040 seconds) than the modern controlled system (0.075 seconds), the maximum percent overshoot of the PID controlled system across all runs is 10.0%, while the maximum overshoot of the modern controlled system is 3.9%. Also, the oscillations observed in the PID controlled system can be harmful to hydraulic equipment, making the smoother response of the modern controlled system more favorable. The step responses of the PID controlled system and the modern controlled system with varying load valve areas are shown in Figure 46 and Figure 47, respectively.

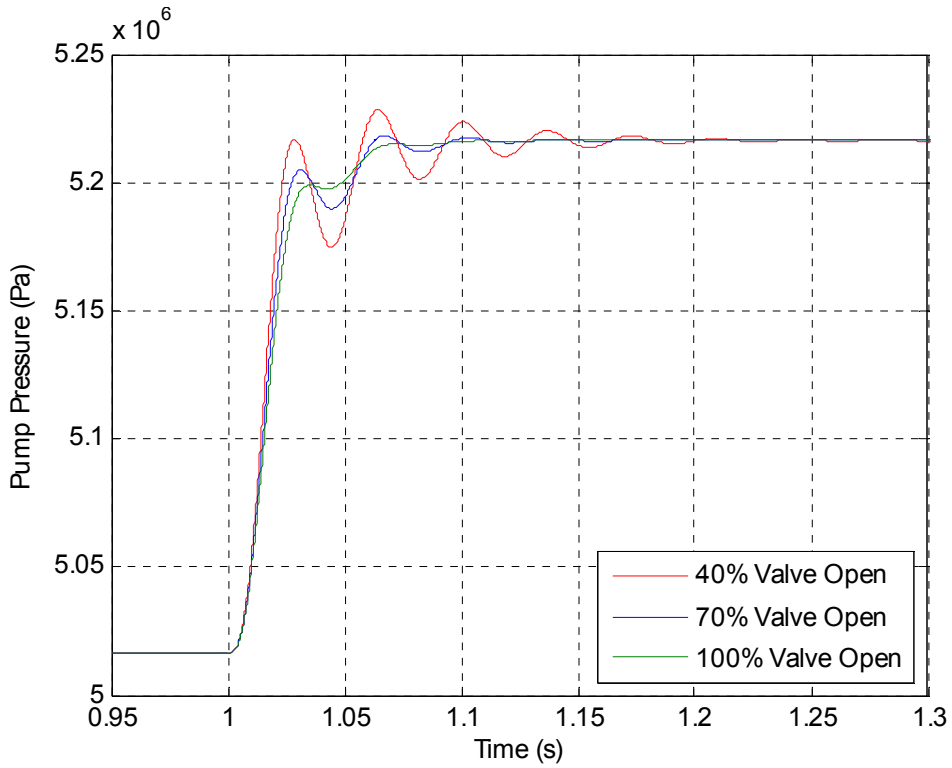

Figure 46. Variation of the PID controlled system for changing load valve area

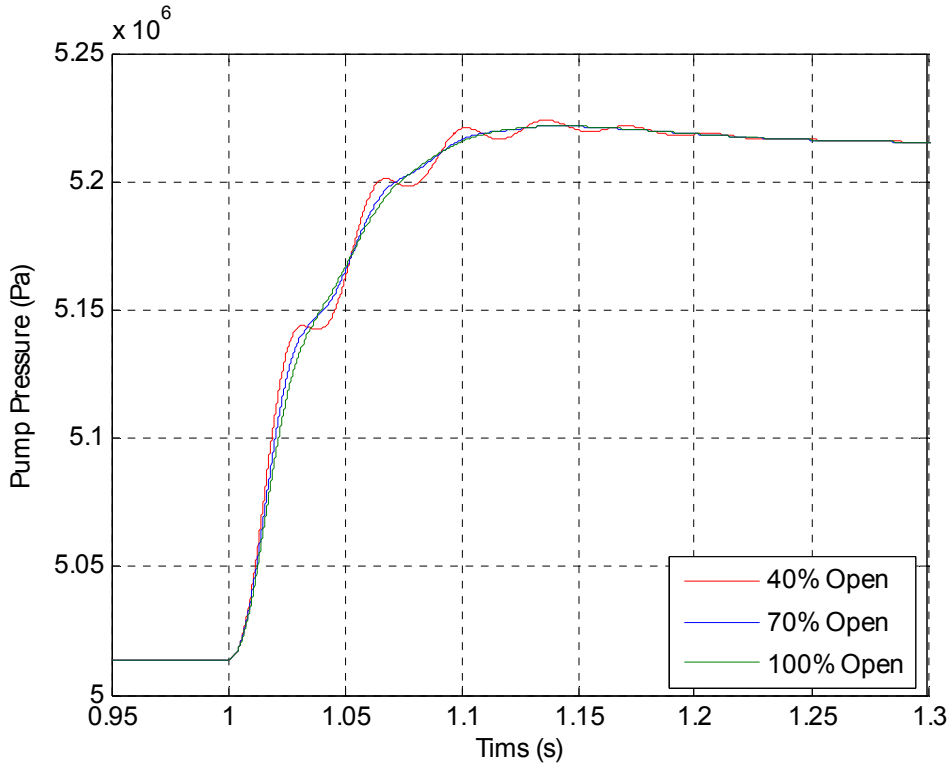

Figure 47. Variation of the modern controlled system for changing load valve area

Once again, the rise time of the PID controlled system is faster (0.040 seconds) than the modern controlled system (0.065 seconds). The maximum overshoot of the PID controlled system over all trials is 6.05% and only 3.15% for the modern controlled system. Oscillations similar to these observed in the bulk modulus trials are seen again in the load valve trials.

A comparison of disturbance rejection in the two controlled systems is shown in Figure 48. At time t = 1 second, the load valve area is instantaneously increased as noted earlier, and at time t = 2 seconds, the load valve area is reduced instantaneously.

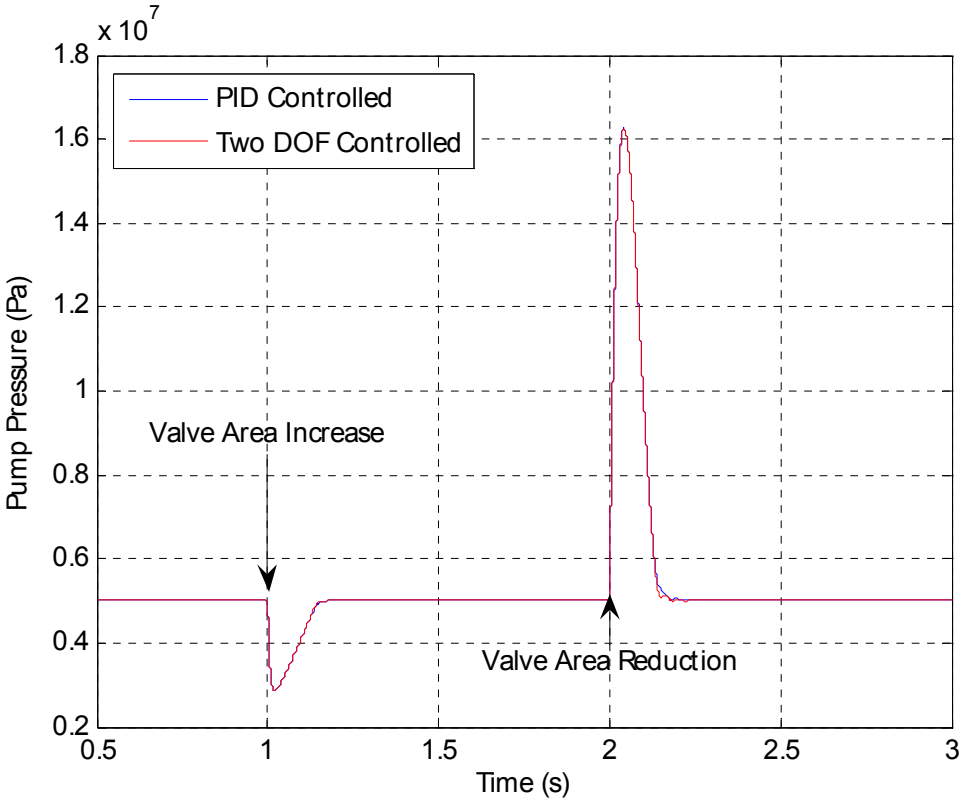

Figure 48. Comparison of disturbance rejection between the two models

The two system responses shown in Figure 48 are nearly identical, suggesting that the modern control scheme does not improve upon the PID controlled system response to large load valve disturbances. The plot of normalized control valve input from both models during the disturbance trial is shown in Figure 49. Both controllers attempt to actuate the control valve beyond its boundaries, saturating it at either its maximum or minimum position. This indicates that the large disturbance rejection response of the system is dictated by the mechanical properties of the system, rather than its controller.

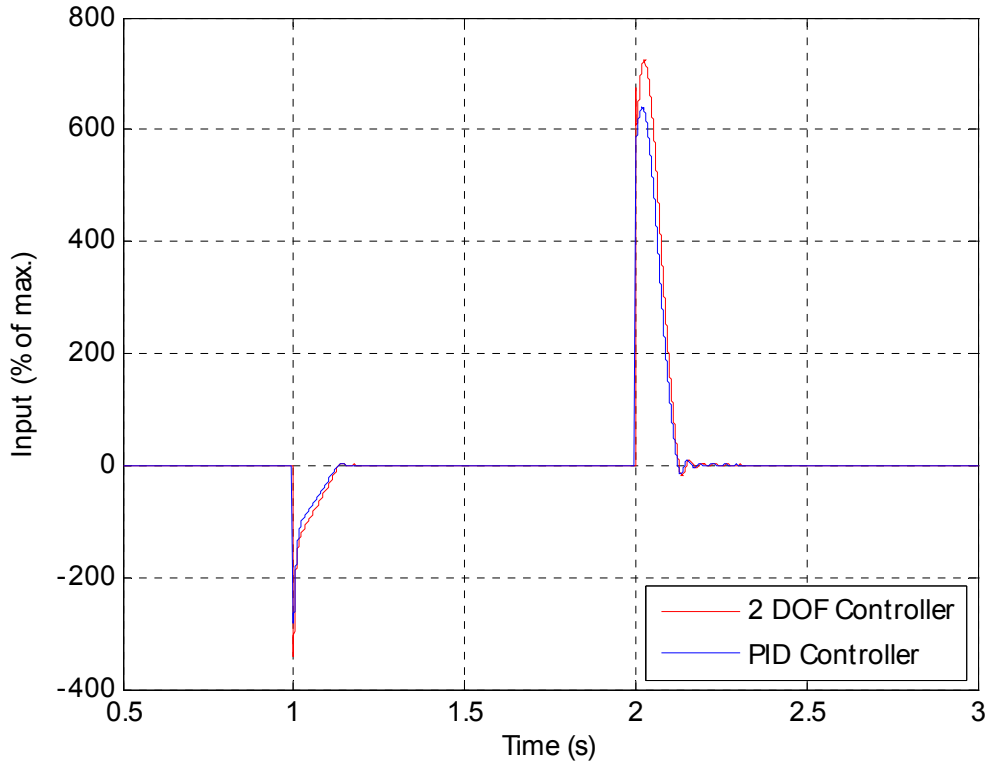

Figure 49. System input comparison between the two controllers during disturbance trial

7.3 Time Domain Analysis Conclusions

Overall, the two degrees-of-freedom controlled system showed better robustness to parameter variation than did the PID controlled system. While the time response of the PID controlled system was faster, it was characterized by greater oscillation and overshoot than observed in the modern controlled system response.

Both the classically controlled system and the modern controlled system produced nearly identical results during the large perturbation trial. The similarity of the two responses suggests that the response of this hydraulic pump to large fluctuations in load valve area is determined by the attributes of the mechanical system, rather than the control method chosen.

Chapter 8

CONCLUSIONS

8.1 Overview

It can be seen from the results of this project that modern control can effectively increase the robustness qualities of a control system on a hydraulic pump. By comparing Figures 44 - 47, the variance of the system response due to parameter fluctuation was decreased by using a two degrees-of-freedom H_∞ controller, rather than a classical PID controller. These time domain results were predicted by the robustness analysis performed in the frequency domain. The robustness test results shown in Table 4 concluded that, while the modern control design would not improve performance characteristics over the classical control scheme, the robust stability of the system was improved by 34%.

While the two degrees-of-freedom H_∞ control design allowed for greater robustness to parameter fluctuation, the large disturbance response of the system was unaffected by the choice of control method. The system output comparison between the two control schemes seen in Figure 48 shows that the response due to a large change in load valve area is nearly identical across both controller designs. The notion that controller saturation is to blame for this effect is confirmed with the control valve input comparison shown in Figure 49.

The advantages of pursuing a structured uncertainty model rather than an unstructured uncertainty model were shown in Chapter 3. By comparing the unstructured uncertainty description shown in Figure 20 and the structured

uncertainty description shown in Figure 23 and Figure 24, it can be concluded that analyzing the uncertainty in each system component separately allows for a much less conservative control scheme. In fact, the peak uncertainty calculated by the unstructured model was found to be 15 times greater than the peak uncertainty calculated by the structured model.

8.2 Limitation of H_∞ Control

While the advantages of using modern control methods and analysis have been outlined in this project, the drawbacks of such concepts have not. The main limitation of H_∞ control design is the fact that it yields high-order controllers. These controllers require increased processing capabilities during design and analysis, but more importantly, increased processing capabilities from the onboard computer running the controller in real-time.

Also, in terms of hydraulic pumps specifically, unwanted integral terms in high-order controllers can cause excessive overshoot effects when the system response is saturated. This integrator "wind-up" effect can be observed in a hydraulic pump response for large, sudden changes in commanded discharge pressure when integrator terms are present in the controller.

8.3 Scope of Future Work

While the time domain simulations shown in Chapter 7 are encouraging, they were not performed using a hydraulics-specific software package. The utilization of the mechanical simulation program, *Dynasty*, would perhaps allow for more accurate

results. This program would be able to assess the feasibility of using the high-order controllers derived on currently available signal processing equipment. Also, analysis of the linear and nonlinear models using *Dynasty* to investigate which combination of varying parameters might cause an unstable system would be helpful.

Once extensive simulation testing was performed using these modern control methods, hardware testing could begin. The results of hardware testing would be the final and most important assessment of the viability of these control methods.

One major concern of hydraulic pump control is instability due to control valve capabilities. Previously, smaller control valves have been used to actuate hydraulic swash-plate pumps, since slow response is desired for enhanced controllability. However, the use of larger control valves would allow for larger flow rates into the control chamber, yielding faster pump pressure responses. Modern controllers could assure greater stability than classical controllers might, given this higher flow rate.

Appendix

MATLAB CODE FOR TWO DEGREES-OF-FREEDOM CONTROL DESIGN

The following code creates a two degrees-of-freedom modern controller for the plant *G*. The program is a stand alone unit, loading parameters from exterior sources when necessary. The first step of the two degrees-of-freedom control design is to establish a reference model with the desired system response parameters.

```
wn=4*2*pi;
zeta =0.8;
Tref11 = tf([wn^2],[1 2*zeta*wn wn^2]);
Tref=ss(Tref11);
```

A desired natural frequency of 4 Hz and damping ratio of 0.8 are chosen. Next, the PID controller designed for performance is established, which will help form the shaped plant.

```
K_PID=tf([.008 .5],[1/10000 1]);
W1=K_PID;
W1_ss=ss(W1);
```

The linear plant *G* is loaded into the program from an external source and stored.

```
load linear_plant_711;
Gs=G;
clear G;
```

Next, the shaped plant G_{shaped} is formed by combining W_1 and the open-loop plant. Also in this step, the shaped plant and reference model are converted into the "packed" format, which combines the *A, B, C,* and *D* matrices of a state-space representation into a single matrix for simpler analysis.

```
G_shaped = Gs*W1;   % shaped plant
Gs_pck = pck(G_shaped.a, G_shaped.b, G_shaped.c, G_shaped.d);
Tref_pck = pck(Tref.a, Tref.b, Tref.c, Tref.d);
```

With the shaped plant and reference model in the correct form, the calculation of the controller gains can begin. The model-matching factor ρ is first chosen, then the

Matlab utility *hinf2dof.m* is used to calculate the controller gains K_1 and K_2, both contained within the variable *K_2dof*.

```
rho=1.1;
K_2dof_pck=hinf2dof(Gs_pck, Tref_pck,rho);
[Ak2dof,Bk2dof,Ck2dof,Dk2dof]=unpck(K_2dof_pck);
K_2dof=ss(Ak2dof,Bk2dof,Ck2dof,Dk2dof);
```

Once the controller gains are "unpacked" and returned to a standard state-space representation, model-order reduction can begin. The *Matlab* utility *sresid.m* is used to reduce the order of the controller to 6th order. This process once again requires the controller to be in the "packed" form.

```
sysred=pck(K_2dof.a,K_2dof.b,K_2dof.c,K_2dof.d);
sysd=strans(sysred);
sysr=sresid(sysd,6);
[asysr,bsysr,csysr,dsysr]=unpck(sysr);
K_2dof=ss(asysr,bsysr,csysr,dsysr);
```

The separate controller gains K_1 and K_2 can now be individually extracted from *K_2dof*.

```
K1=K_2dof(:,1); K2=K_2dof(:,2);
```

Next, the scaling matrix, W_i, can be defined. Recall that this matrix allows for reference model matching at steady-state, reducing the steady-state error of the system.

```
Hinf2dof_cl=series(K1,feedback(G_shaped,-K2));
Wi_2dof=inv(dcgain(Hinf2dof_cl))*dcgain(Tref);
```

The controller model can now be assembled from the calculated matrices and values. The controller is of a two-input, single-output architecture, defined by the following code:

```
Two_DOF_Controller = minreal([-K2*W1_ss Wi_2dof*K1*W1_ss]);
```

Next, the performance weighting characteristics can be established. The maximum allowable high frequency error is 200%, the desired bandwidth is 2 Hz, and the allowable steady-state error is 5%. These values are then entered into the performance weighting transfer function, w_p.

```
M_1 = 2;
bandwidth_1 = 2*pi*2;
A_1 = .05;
w_p = tf([1/M_1 bandwidth_1], [1 bandwidth_1*A_1]);
```

The displacement model and the load valve model along with the uncertainty descriptions must be introduced to the program.

```
load V_G
V=G;
clear G

load G_G

load w_g
w1 = WaSS;
clear WaSS

load w_v
w2=WaSS;
clear WaSS
```

Next, the control valve dynamic approximation must be added to the system. Along with this addition, the displacement model must be divided into two separate state-space representations: one with the control valve current as an input and the other with the pump discharge pressure as its input.

```
control_valve = tf([6750/.0623],[1 28.98/.0623 6750/.0623]);

D1 = ss(G.a,G.b(:,1),G.c,0);
D1 = ss(control_valve)*D1;
D2 = ss(G.a,G.b(:,2),G.c,0);
```

With all of the plant models, uncertainty descriptions, and performance weighting characteristics loaded into the program, the generalized plant, P, can be assembled.

```
den=1-D2*V;
```

```
P=[ w1*V*D2/den     w1*D2/den       0       w1*D1/den;
    w2*V/den        w2*V*D2/den     0       w2*V*D1/den;
    -V*w_p/den      -V*D2*w_p/den   w_p     -D1*V*w_p/den;
    0               0               1       0;
    -V/den          -1/den          1       -D1*V/den ];
```

The generalized plant can then be combined with the controller using the lower-linear fractional transformation routine *lft.m*. Once this is accomplished, the robustness characteristics of the controlled system can be analyzed graphically.

```
N=lft(P,Two_DOF_Controller);

w=logspace(-2,4,300);

figure
sigma(N(3,3),w)
title('Nominal Performance, 2DOF')

M=N(1:2,1:2);

figure
sigma(M,w)
title('Robust Stability, 2DOF')

figure
sigma(N,w)
title('Robust Performance, 2DOF')
```

REFERENCES

[1] Njabeleke, I.A.; Pannett, R.F.; Chawdhry, P.K.; Burrows, C.R., 1997, "H_∞ Control in Fluid Power," *IEE Colloquium on Robust Control: Theory, Software and Applications*, pp. 7/1-7/4

[2] Shamma, J. S., 1994, "Robust Stability with Time-Varying Structured Uncertainty," *IEEE Transactions on Automatic Control*, **39(4)**, pp. 714-724

[3] Zhang, R., Alleyne, A. and Prasetiawan, E., 2002, "Modeling and H_2/H_∞ Control of an Earthmoving Vehicle Powertrain," Journal of Dynamic Systems, Measurement, and Control, **124**, pp. 625-636.

[4] Fales, R. C., White, W. N., and Kelkar, A. G., 1996, "A Hydraulically Actuated Compound Pendulum," *IEEE International Conference on Control Applications*, Dearborn, MI, pp. 426-431.

[5] Fales, R. C., and White, W. N., 1999, "Control of a Double Inverted Pendulum with Hydraulic Actuation: A Case Study," *American Control Conference,* San Diego, CA, pp. 495-499.

[6] Hongliu Du and Manring N. D., 2001, "A Single-Actuator Control Design for Hydraulic Variable Displacement Pumps," *Proceedings of the 2001 American Control Conference,* **(6)** pp. 4484-4489.

[7] Skogestad, S., and Postlethwaite, I., 1996, *Multivariable Feedback Control: Analysis and Design,* John Wiley and Sons, New York.

[8] Dean, P., Bax, B., and Fales, R., 2006, "Reliable Hydraulic Control System Design," University of Missouri – Columbia, internal document.

[9] Bax, B., 2006, "Applying and Analyzing Robust Modern Control on Uncertain Hydraulic Systems," University of Missouri – Columbia, internal document.

[10] Skogestad, S., 1995, "coprimeunc.m," "Matlab Files for MULTIVARIABLE FEEDBACK CONTROL." http://www.nt.ntnu.no/users/skoge/book/2nd_edition/matlab_m/matfiles.html#c9. June 1, 2006.

[11] Skogestad, S., 1995, "hinf2dof.m," "Matlab Files for MULTIVARIABLE FEEDBACK CONTROL." http://www.nt.ntnu.no/users/skoge/book/2nd_edition/matlab_m/matfiles.html#c9. June 1, 2006.